uOttawa

L'Université canadienne
Canada's university

FACULTÉ DES ÉTUDES SUPÉRIEURES ET POSTOCTORALES

uOttawa

L'Université canadienne
Canada's university

FACULTY OF GRADUATE AND POSDOCTORAL STUDIES

Vasilisa Flippenko
AUTEUR DE LA THÈSE / AUTHOR OF THESIS

M.Sc. (Chemistry)
GRADE / DEGREE

Department of Chemistry
FACULTÉ, ÉCOLE, DÉPARTEMENT / FACULTY, SCHOOL, DEPARTMENT

Oxygen Uptake Studies of Organic and Inorganic Oxidations
TITRE DE LA THÈSE / TITLE OF THESIS

J.C. Scaiano
DIRECTEUR (DIRECTRICE) DE LA THÈSE / THESIS SUPERVISOR

CO-DIRECTEUR (CO-DIRECTRICE) DE LA THÈSE / THESIS CO-SUPERVISOR

J. Pezacki

M.DeRosa

Gary W. Slater
Le Doyen de la Faculté des études supérieures et postdoctorales / Dean of the Faculty of Graduate and Postdoctoral Studies

Oxygen Uptake Studies of Organic and Inorganic Oxidations

Vasilisa Filippenko

Thesis submitted to the

Faculty of Graduate and Postdoctoral Studies

in partial fulfillment of the requirements for the degree of

Master of Science

Specialization in Chemistry

in the Ottawa-Carleton Chemistry Institute

Department of Chemistry, University of Ottawa

Université d'Ottawa · University of Ottawa

Candidate

Vasilisa Filippenko

Supervisor

Professor J. C. Scaiano

Your file Votre référence
ISBN: 978-0-494-65994-6
Our file Notre référence
ISBN: 978-0-494-65994-6

To my mother.

With deep love and gratitude,

for always being there.

Abstract

The investigations in this thesis deal with two types of very different oxidations. The first study follows our groups' discovery of a new and unusual class of antioxidants, where the actual antioxidant is, paradoxically, a carbon-centered radical. The radical precursors are dimer molecules that, upon heating, dissociate to form two persistent carbon-centered free radicals, unreactive towards oxygen. These radicals act as chain-breaking antioxidants by rapidly reacting with peroxyl radicals that participate in propagation of autoxidation chain reactions. The solvent effects on antioxidant activity of one of these antioxidants, the HP-136 dimer, has been assessed in a range of solvents of varying hydrogen bond accepting ability, by the Inhibited Oxygen Uptake (IOU) method. The HP-136 dimer was found to show far less solvent effect on antioxidant activity than a representative phenolic antioxidant.

In the second part of the thesis, the process of copper nanoparticle (CuNP) oxidation is explored, with a goal of developing new strategies for CuNP stabilization under air. It was found that CuNP oxidize to form Cu^{2+} as the major product, in a process that involves oxygen uptake. L-ascorbic acid was found to be a sacrificial stabilizer of CuNP, and a mechanism of CuNP stabilization by ascorbic acid is proposed.

Acknowledgements

I could not ask for a better research supervisor than Tito Scaiano. In addition to being a brilliant researcher and a talented leader, he is a beautiful person, and is very kind. Thank you so much for your support, encouragement and patience! I feel truly lucky, and proud to be part of your group.

I am also extremely fortunate to have worked with Mathieu Frenette, whose project I continued when just starting my graduate studies. It was a blessing that you were there! I cannot thank you enough for all your help, thoughtfulness and patience. Your explanations made learning chemistry radically enjoyable! It was a great pleasure working with you.

I would like to thank Keith Ingold for valuable research discussions, and also for the water skiing trips! It was an honour to meet you and a pleasure to talk to you.

I would like to acknowledge and thank Ross Barclay for designing the oxygen uptake instrument – this project would not be possible without your generous gift.

I would especially like to thank Natalia Pacioni for all the help, advice, valuable discussions and encouragement – it was a great pleasure working with and talking to you! Also, I would like to thank Nathalie Presseau – I enjoyed working and learning with you very much. I am very thankful to Michel Grenier all the help, and

particularly for connecting the oxygen uptake apparatus to a computer, which saved me a considerable amount of time. Also, a big thank you to Betty Yakimenko for taking such good care of all of us!

I had the most enjoyable graduate school experience imaginable, and the people in the Scaiano group are the ultimate reason for that. I will cherish the memories of all the fun times and jokes we shared (my English and Spanish vocabulary improved considerably). I would like to acknowledge everyone who I have worked with throughout the years: Kathy-Sarah Focsaneanu, Marie Lafferiere, Colleen Sutton, Larisa Mikelson, Vincent Maurel, Belinda Heynes, Mark Perry, Steve MacGuire, Robert Godin, Kathy McGilvray, Jessie Blake, Paul Billone (and the EPR), Alexis Aspee, Laetitia Rene-Boisneuf, Eve Heafey, Matthew Yorke, Matthew Decan, Liliana Jimenez, Maria Gonzalez-Bejar (yellow blue bus!), Marta Liras, Andrea Pardoe, Kevin Stamplecoskie, Jose-Carlos Ferreira, Geniece Hallett-Tapley, Charles-Oneil Crites, Luca Maretti, Julie Park, Erika Wee and Emilio Alarcon.

I am also very glad that I had the opportunity to participate in the Let's Talk Science program. I am happy to have shared it with Laetitia and Andrea (I will miss you, girls!). This was an unforgettable experience, which I hope to continue even after I finish graduate school.

Finally, I would like to thank my family – Tatiana and Kyrill Reznikov, and my grandmother. I love you so much.

Table of Contents

List of Figures

List of Schemes

List of Tables

List of Abbreviations

α-tocopherol = main component of Vitamin E

μL = microliters

μM = micromolar

τ = inhibition period

A = pre-exponential factor

A_{max} = maximum absorption

AC = alternating current

AgNP = silver nanoparticles

AIBN = 2,2'-azo-bis-isobutyronitrile

AuNP = gold nanoparticles

Cu^{+} = copper (I)

Cu^{2+} = copper (II)

CuNP = copper nanoparticles

$CuSO_4$ = copper sulfate

DAQ = Data Acquisition System

DNA = deoxyribonucleic acid

E_a = activation energy

EPR = Electron Paramagnetic Resonance

HP-136 = CIBA's Irganox HP-136 ®

HOO• = hydroperoxyl radical

HO• = hydroxyl radical

H_2O_2 = hydrogen peroxide

$h\nu$ = photon of light

I-2959 = CIBA's Irgacure 2959 ®

I-907 = CIBA's Irgacure 907 ®

IOU = Inhibited Oxygen Uptake

k_i = rate constant of initiation

k_{inh} = rate constant of inhibition

k_p = rate constant of propagation

k_t = rate constant of termination

L = liter

LED = Light Emitting Diode

M = moles per liter

mM = millimolar

mol = moles

m°C = millidegrees Celsius

O_2 = dioxygen, molecular oxygen

$^1O_2$ = singlet oxygen

$O_2^{-\bullet}$ = superoxide radical

PMHC = 2,2,5,7,8-pentamethyl-6-hydroxychroman (Vitamin E analogue)

PTFE = poly(tetrafluoroethylene)

PVP = polyvinylpyrrolidone

Redox = oxidation-reduction reaction

RO• = alkoxyl radical

ROO• = peroxyl radical

ROS = Reactive Oxygen Species

RH = oxidizable substrate

R_i = rate of initiation

Ru = Ruthenium

s = second

SEM = Scanning Electron Microscope

SPR = Surface Plasmon Resonance

T = temperature

TEMPO = 2,2',6,6'-tetramethylpiperidine-N-oxide (free radical)

UV = ultraviolet

V = volts

V-601 = dimethyl 2,2-azobis(isobutyrate)

Vitamin C = L-ascorbic acid

1 Introduction

1.1 Studies of Oxidations

Oxidation reactions are all around us – yellowing of many materials such as paper, combustion, and cellular respiration of living organisms are just some examples of the diverse processes involving oxidations. A reaction is defined as being oxidation-reduction, or "redox", if any element undergoes a change in oxidation number during the course of the reaction[1]. The oxidation number refers to an element's oxidation state: if the number increases, the element is oxidized, and if it decreases – the element is reduced. Often, but not always, redox reactions involve electron transfer, where an element that loses electrons is oxidized, and one that gains electrons is reduced. In organic chemistry, one could also look at redox reactions from the point of view of hydrogen- and oxygen-atom content. Usually, oxidation of an organic molecule corresponds to increasing its oxygen content or decreasing its hydrogen content[1] (Scheme 1.1). The opposite is usually true for a reduction process.

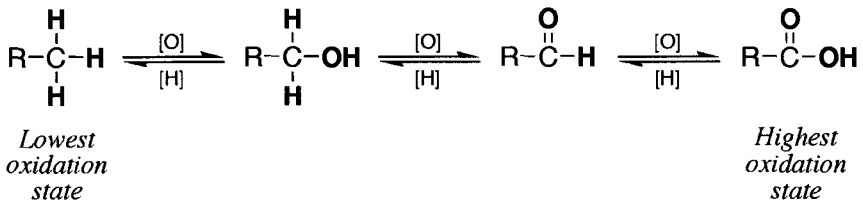

Scheme 1.1 General degrees of oxidation of organic molecules.

Unaided oxidation by O_2 is slow because of its unusual electronic configuration. In its normal, unexcited energy state – the ground state – dioxygen exists as a triplet, whereas most molecules in their ground states are singlets. Hund's rule explains this phenomenon – ground state O_2 has two degenerate molecular orbitals that are half-occupied in which the electrons arrange in parallel spins. As a result O_2 is paramagnetic, as illustrated by the Molecular Orbital diagram of ground state dioxygen in Scheme 1.2. In the Lewis structure, ground-state molecular oxygen can be simplistically drawn as a biradical[2,3].

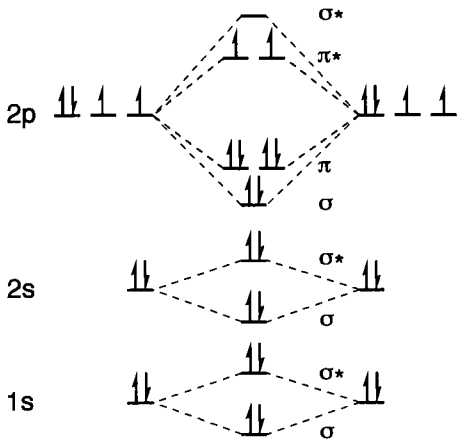

Scheme 1.2 Molecular Orbital diagram of ground state O_2. Note that this molecule has a triplet electronic configuration.

In fact, if O_2 did not exhibit this unusual property, we would not exist, because dioxygen in its singlet state is highly reactive with other singlet-state molecules, and so living organisms would be oxidized very quickly. For triplet dioxygen, on the other hand, reactions with singlet-state molecules are *spin-forbidden*, and therefore ground state O_2 is much less reactive with other singlet-state molecules. However,

ground state O_2 is usually very reactive with molecules in their doublet state, such as radicals. Radical reactions are often closely linked to the O_2-incorporating oxidations.

In oxidations involving reactions with molecular oxygen, monitoring the uptake of O_2 gas provides a convenient tool for measuring oxidation rates and rate constants. The instrument employed in this thesis is the Oxygen Uptake Apparatus. In this work, measuring oxygen uptake was a central technique for studying two very different types of oxidations.

At first, the very well established Inhibited Oxygen Uptake (IOU) method was used to study antioxidant activity of a novel antioxidant, the HP-136 dimer. This study is presented in Chapter 2. The oxygen uptake apparatus is traditionally used in the analyses of antioxidant activity of compounds, since monitoring oxygen uptake is the most direct method of assessing antioxidant activity, although the method is relatively time-consuming.

The second type of oxidation studied was that of copper nanoparticles (CuNP), which is presented in Chapter 3. For the oxygen uptake apparatus, this is a novel application for the instrument, and it was quite exciting to see the adaptation of the traditional instrumentation, that has been used for decades, for newly emerging applications, such as nanochemistry.

1.2 Oxygen Uptake Apparatus

The oxygen uptake apparatus was a gift to the Scaiano group from Dr. Ross Barclay of Mount Allison University (New Brunswick), a renowned chemist in the field of radical chemistry. Dr. Barclay built this apparatus himself, in the late 1970's.

The instrument works by sensing the difference in pressure between two cells – a sample and a reference. Hollow springs connect the two cells to a pressure transducer, which is the key element of the instrument (Figure 1.1). The transducer consists of two chambers separated from each other by a metal membrane. The hollow springs connect each cell to one of the chambers. If the pressure in the chambers (and cells) is not the same, the membrane bends, and thus detects this pressure difference. This slight change in shape is, in turn, converted to an electrical output signal, in volts (V).

To run an experiment, the desired reaction is set up in the sample cell. In general, the composition of the sample and reference cells must be identical, except for one distinguishing parameter, such as the presence of initiator (present in sample cell, but not reference). For example, if an oxidation reaction is taking place, oxygen is being consumed only in the sample cell, thus creating the pressure difference being measured by the instrument.

The electrical signal from the pressure transducer is translated to a chart recorder pen. Essentially, the data output is the chart recorder pen writing on paper.

Two parameters control the data output; the speed of the recording, and the sensitivity. The speed refers to how fast the paper moves – typically 12 cm/h for my experiments. The sensitivity of signal detection can be as high as 1 volt per scale (V/scale). The scale is the width of the chart recorder paper (25 cm). Depending on the experiment, the sensitivity of the apparatus may need to vary. In most of my experiments, a sensitivity of 5 V/scale is used. Thanks to our laboratory technician, Michel Grenier, the oxygen uptake data is also recorded digitally. Michel wrote a program using Labview 8.5 software, and connected the computer to the apparatus through a Data Acquisition System (DAQ), purchased from National Instruments, such that the data output is collected on the computer in real time. This was of invaluable help, which saved hours (maybe days) of experimental data processing! Prior to this, a ruler had to be used. Although the data is collected on a computer, I still found it very useful to also record the experiment with the chart recorder, for quick analysis, record-keeping and estimation purposes.

It is important to remember that the kinetic data obtained by this method is relative, since all the pressure difference measurements of the sample reaction are done relative to the reference cell pressure.

Alternate techniques for detecting changes in oxygen partial pressure include fluorescent sensors. For example, the FOXY probes, manufactured by Ocean Optics, use fluorescence of Ruthenium (Ru) complexes to measure partial pressure of oxygen gas[7]. They work by exciting the Ru probe with LED light and measuring

Ru fluorescence quenching, which relates to the concentration of oxygen. If oxygen is present, Ru fluorescence is quenched faster. These probes are, however, mostly designed for measurements in aqueous solutions, and are not suitable for our experiments.

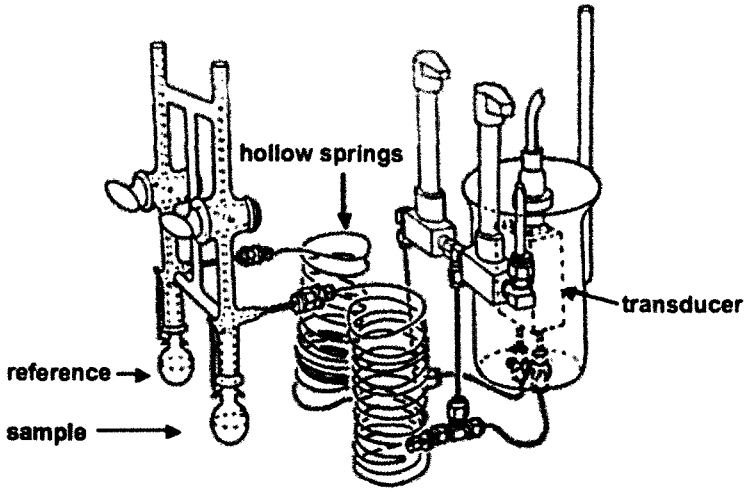

Figure 1.1 Schematic diagram showing the main parts of the Oxygen Uptake Apparatus.

There are a number of details to address in our oxygen uptake experiments. It is essential to keep the temperature very uniform throughout the experiment because variations in temperature lead to large fluctuations in the pressure detected. For this reason, the apparatus hosts a large waterbath in which the cells are kept, with insulating walls and a stirrer. The desired water temperature is set manually and is maintained with a very sensitive (± 5 millidegree Celsius, m°C) automatic temperature controller. The cells in the waterbath are attached to a

vigorous shaker, ensuring that the diffusion rate of gas throughout the sample is fast, and is never a rate-limiting factor. Also, the cells are especially designed, and have a splashguard (Appendix). Prior to an experiment, the apparatus should be vacuumed down, to ensure that no solvent has condensed in the hollow tubing leading from the cells to the transducer. Once clean, equilibration with solvent should be done overnight to allow solvent vapour to diffuse throughout the hollow tubing to the tranducer chambers. The next morning, a baseline and pressure check should be performed to make sure the apparatus is working properly. There are two knobs on top of the apparatus – one controls whether the system is closed or open to surroundings, and the other controls the connection between the reference and sample cell environments. During an experiment, the cells are isolated from each other, and the system is closed to the surroundings. Further details are found in the Experimental Details section.

Before any experiments can be performed, however, a calibration factor for the cells must be determined.

1.3 Determination of Calibration Factor for Sample Cell

To be able to measure the moles of gas consumed or released in a reaction, it is necessary to be able to convert the electrical output of the instrument into moles of gas. Each particular cell used in the apparatus has a unique calibration factor, since each one has a unique volume, and therefore, the sensing of the pressure transducer will vary from cell to cell.

The basic principle for determining the calibration factor is to initiate an autoxidation with a known rate and detect the consumption of oxygen with the oxygen uptake apparatus. Remember that what is actually detected is the electrical signal from the change in shape of the pressure transducer membrane as the pressure of the sample cell changes with respect to the reference cell. Thus, we are seeking a conversion factor from electrical units (volts, V) to amount of gas (moles, mol), in this case oxygen.

We initiated an autoxidation reaction where the oxygen consumed could be calculated using equation (1):

$$\frac{d[O_2]}{dt} = -\frac{k_p[RH]R_i^{1/2}}{(2k_t)^{1/2}} \qquad (1)$$

where $d[O_2]/dt$ is the rate of oxygen consumption, k_p and k_t are rate constants for propagation and termination, respectively, [RH] is the concentration of the autoxidizing substrate and R_i is the rate of initiation. To use this equation, a suitable

substrate must be chosen for which the k_p and k_t are known, and for our experiments we chose the very well-established styrene autoxidation. In this case, the reaction was initiated with AIBN in pure styrene[4], which has k_p of 41 $M^{-1}s^{-1}$, and k_t of 4.2 x 10^7 $M^{-1}s^{-1}$. Thus, the only parameter that we do not know from equation (1) is R_i. A correction for N_2 evolution from AIBN was made. However, since AIBN is required only for initiation of chain reaction, after which the chain propagation continues independently, only a small amount of AIBN is used. Therefore, the N_2 produced was found to be negligible when compared to the levels of oxygen uptake.

To measure R_i, we inhibited the autoxidation reaction by injecting a vitamin E analogue, PMHC (2,2,5,7,8-pentamethyl-6-hydroxychroman), which has a known stoichiometric factor, *n*=2. Injection of PMHC yields an oxygen uptake curve with a very well defined inhibition period, τ. The inhibition period is the time required for the antioxidant to be consumed. During this time the rate of oxygen uptake decreases, and, once the antioxidant is used up, the autoxidation rate returns to the uninhibited level. One can think of this experiment as a free radical titration where PHMC is consumed by propagating peroxyl radicals. R_i is then determined using the relationship in equations (2):

$$R_i = \frac{n[PMHC]}{\tau} \qquad (2)$$

We then compared our measured R_i to a theoretical value which was obtained from equation (3), where *e* is the efficiency of initiation (*e*=0.64 for AIBN),

and k_i is the rate constant of initiation for AIBN, and is determined from the Arrhenius equation (4):

$$R_i = 2ek_i[AIBN] \quad (3)$$

$$k_i = Ae^{-\frac{E_a}{RT}} \quad (4)$$

In equation (4), A is the pre-exponential factor ($1.58 \times 10^{15}\ s^{-1}$) and E_a is the activation energy (30.8 kcal/mol)[5]. R and T are the ideal gas constant and temperature in Kelvin, respectively. As expected, the measured R_i was in good agreement with the values calculated from equation 3.

With the obtained R_i, all the information is now available to calculate $d[O_2]/dt$, which yields oxygen uptake rate in concentration units in time, M/s, and it is necessary to take into account the volume of the reaction mixture for an answer in moles of O_2 consumed per second (mol/s).

The uninhibited autoxidation plot from the oxygen uptake apparatus exhibits a straight line, with rate of voltage change, dV/dt, as the slope. All that is left to obtain the calibration factor is to equate dV/dt with the d(mol O_2)/dt. The calibration factor calculated for two cells are given in Table 1.1.

Table 1.1 Calibration factors obtained by IOU method with styrene autoxidation at 30°C. Values based on three trials (± one standard deviation).

Cell	Calibration Factor
Engraved "S"	**$6.99 \times 10^{-7} \pm 0.09$ moles O_2 / V**
Engraved "iii"	**$5.33 \times 10^{-7} \pm 0.18$ moles O_2 / V**

Note that the calibration factor is for a particular cell only, and each cell used should be calibrated individually. The calibrated cell is used on the sample side, only, since the data output is achieved from the sample cell (i.e. the chart recorder responds to the changes in the sample cell). Of course, the reference cell plays a very important role, as well, and changing the reference cell would affect the data output. For this reason, sets of experiments are performed with the same set of cells. In this case, all the experiments discussed in Chapter 2 were run using cell "S", and a corresponding reference cell. The experiments discussed in Chapter 3 use the cell engraved "iii", and a corresponding reference cell.

Once calibrated, it is possible to reliably measure variations of oxygen pressure corresponding to less than 0.1 μmoles of O_2. In the following chapters, the application of oxygen uptake measurements will be used to investigate the antioxidant activity of "radically different antioxidants" (Chapter 2) and to study the oxidation of "naked" copper nanoparticles (Chapter 3).

1.4 Experimental Details

The following sections describe the oxygen uptake apparatus in considerable detail, possibly more than usually described in a thesis. I have done so to provide a permanent record of the procedures, since this "home made" instrument has no manual. The format closely follows that of the journal *Nature Procedures*.

1.4.1 Instrumental Parts

Labview 8.5 software program, 100 μL, 500 μL and 1 mL gas-tight glass syringes with Teflon Luer lock (Hamilton), rubber septa (Sigma-Aldrich), 10 mL volumetric flasks, glass vials, poly(tetrafluoroethylene) (PTFE) tubing, oxygen uptake cells (see Appendix), vacuum pump (V-500 Buchi Vac), steel needles (22 gauge). Parts for O2 uptake apparatus:

i. Variable reluctance differential pressure transducer, DP15TL (Validyne). AC output.

ii. Universal transducer indicator, CD12 (Validyne). DC output.

iii. Temperature controller, PTC-41 (Tronac Inc.)

1.4.2 Oxygen Uptake Apparatus Controls

There are two knobs on the top of the oxygen uptake apparatus, and each knob can either be in the "open" or "closed" position. A green knob controls the connection between the reference side and sample side of the chamber that is

separated by the pressure transducer. When the green knob is in the "open" (or "balance") position, the passage is open, and so the pressures between the sample and reference sides are equalized. If the green knob is in the "closed" (or "measure") position, the sample and reference sides are isolated from each other, and can have different pressures. The red knob controls the passage leading from the reference side of the chamber to the external environment. In the "open" (or "evacuate") position, the system is in contact with the outside environment. In the "closed" (or "measure") position, the system is isolated.

In general, the apparatus should be in the neutral arrangement as much as possible, where the system is fully open. In other words, both knobs should be "open" ("balance" and "evacuate" positions). In this way, the apparatus cannot be broken. This position should be kept while performing any manipulations with the apparatus (during injections, while removing or inserting cells, when vacuuming down, etc.).

The apparatus is set to "measure" (i.e. both knobs are "closed") when both cells have the desired contents and are ready to be measured. To start the experiment, first close the system to the surroundings (i.e. close the red knob to "measure" position). Then, separate the reference and sample sides by closing the green knob to "measure" position.

To stop the experiment, first balance the pressure on both sides of the transducer chamber (open green knob to "balance" position), and then open the system to surroundings (open red knob to "evacuate" position).

The order for turning the knobs is important to avoid breaking the instrument. Basically, the logic is that you want to separate (and after to equalize) the sample and reference sides while the whole system is closed to the surroundings. The following is one possible scenario for breaking the instrument. For example, if there is a big pressure difference between the sample side and the surroundings, then opening the system to the surroundings before balancing the chambers could cause the delicate membrane in the pressure transducer to snap.

1.4.3 Temperature Control – Water Bath

The water level should be high enough to cover the glass outlets to the hollow green tubing that leads to the pressure transducer chamber. A stirrer in the waterbath ensures homogeneity of the temperature throughout the waterbath, and should be kept on all the time (except when attaching or removing cells).

The temperature of the waterbath is adjusted by manually adding hot and cold water, and monitored with a regular thermometer. Once the desired temperature is set, an electronic temperature controller is turned on to maintain the temperature. "Coarse" and then "fine" control knobs are used to set the temperature sensor. Temperature fluctuations are extremely small – the temperature sensor

detects ± 5 m°C deviations. Thus, the waterbath temperature, as well as the temperature of reaction, is kept very uniform.

1.4.4 Loading Cells and Injecting Sample.

First, attach the cell to the glass cell holder (that leads to hollow tubing and pressure transducer). Place a small amount of vacuum grease on the cell, and secure with metal springs. Then, place the cell into the waterbath and fix to the shaker (Appendix).

For injections into cells, use a syringe with a needle made of PTFE tubing. Ensure no bubbles are present in the tubing. With the apparatus balanced and evacuated (both green and red knobs set to "open" position), open the red stopcock and insert the PTFE needle from the top, until it touches the bottom of the cell. Inject the syringe contents into the cell.

1.4.5 Vacuuming Down Apparatus

The apparatus should be pumped down whenever the solvent system is changed, when the apparatus has not been used for a long time, and when lowering the waterbath temperature. This is done to ensure no trace solvents are present inside. The steps to pumping down are[6]:

i. Open the green and red valves ("balance" and "evacuate" positions).

ii. Load dry, clean cells on apparatus and support them far enough out of the waterbath that the joint from the cell to apparatus is completely out of the water. The red stopcocks above the cells should be closed.

iii. Attach rubber tubing from the vacuum pump to the pumpdown needle valve (located on top of the apparatus, attached to line coming out of the transducer). Make sure the needle valve is closed.

iv. Switch on pump. Make sure the pressure is low enough (1 mm Hg or lower).

v. Very slowly and carefully start opening the needle valve connected to the transducer. While doing this, keep your eye on the demodulator indicator and on the chart recorder pen. It should displace quickly, then return to its original position slowly. If it does not return to the original position, there is a serious blockage, or the knobs have not been fully open and the membrane in the transducer has been damaged.

vi. Pump down the apparatus for at least 3 hours (or overnight).

vii. When finished, close the needle valve. Turn off and remove the vacuum pump.

viii. To release the vacuum, open the needle valve very slowly, once again watching the demodulator indicator and chart recorder pen. The pen

will displace quickly and return to original position. It is important to open the needle valve gradually, until the needle no longer displaces.

1.4.6 Apparatus Equilibration and Baseline

The apparatus must be equilibrated to allow solvent vapours to diffuse throughout the hollow tubes to the pressure transducer. Since the tubes are thin, and diffusion distance quite large, this process takes several hours, and, to be sure, is done overnight. Simply, cells containing pure solvent, or solvent mixture, are loaded, and left overnight, with shaking. Prior to each experiment, a baseline must be recorded, to ensure that the pressure between the sample and reference cells is equivalent. Usually, for baseline measurements, the chart recorder is run at the most sensitive setting – 1 V/scale. A slight drift is acceptable.

1.4.7 Pressure Check

The pressure check is performed after running a baseline, prior to starting the experimental runs, to ensure that the apparatus is functioning properly, and that it is airtight. Particularly, it is done to verify that the calibration factor corresponds to the measured one. Essentially, the pressure check is another, but less sophisticated, way to determine the calibration factor. For the pressure check, the cells are loaded into the waterbath, and are either clean and dry, or contain identical volumes of pure solvent. Use a clean, empty 100 μL syringe to remove/inject fixed volumes of air into the cell in the following manner:

i. Load cells.

ii. Pierce the syringe needle through the rubber stopper on the cell holders.

iii. Set both knobs are set to "measure" (first red, then green). The system is now closed to the surroundings and the sample and reference environments separated.

iv. Set the sensitivity of the apparatus to 5 V/scale.

v. Open the red stopcock leading to the sample cell.

vi. Remove a fixed volume of gas from the cell (eg: 70 μL). The chart recorder pen will move a fixed amount, and should be stable. If the needle starts moving back before you move the syringe plunger, the rubber septum is likely not airtight, and should be changed.

vii. Move the chart recorder paper a little bit to mark the spot that the syringe reached.

viii. Inject the air from the syringe back into the cell. The chart recorder pen will move back to its original position. Mark this spot as well, by moving the chart recorder paper slightly.

ix. Repeat steps v-vii several times. The pen should move precisely to the same position each time the same volume is removed/re-injected.

x. Also, repeat several times by injecting other volumes. For example, I usually inject 3x70 μL, 3x50 μL, and 3x30 μL.

To calculate the calibration factor, use a ruler to measure the distance that the pen moves when a volume of air is injected. Calculate the calibration factor using the equations below:

$$Volts = (length) \times (sensitivity) \div (scale) \quad (5)$$

$$moles\ of\ O_2 = \frac{PV}{RT} \quad (6)$$

$$Calibration\ Factor = \frac{moles\ of\ O_2}{Volts} \quad (7)$$

where equation (6) is the ideal gas law. For example, if the length that the pen travels is 19.3 cm when 70 μL of air is injected at 30°C, the calibration factor is 7.29 x 10^{-7} mol O_2 / V, by the following calculations:

$$Volts = (19.3\ cm) \times (5\ V/scale) \div (25\ cm/scale)$$

$$moles\ of\ O_2 = \frac{(101.35\ kPa)(0.00007\ L)}{(8.314\ JK^{-1}mol^{-1})(303.15\ K)}$$

1.4.8 Calibration Factor Determination using Styrene Autoxidation

AIBN (final concentration ~42 mM) was injected to initiate autoxidation of 2 mL styrene in the sample cell, at 30°C. The reference cell contained pure 2 mL styrene. Constant, uninhibited oxygen uptake rate was measured, resulting in a

straight line. The autoxidation was inhibited by injecting 30 μL stock solution of PMHC for a final sample concentration of ~7 μM. Oxygen uptake rate was measured to yield a curve, with a clearly defined inhibition period. The intersection of trendlines from the inhibited and uninhibited regions of the curve indicates the inhibition period, τ (Figure 1.2). Two additional trials were done by performing consecutive PMHC injections after the PMHC was consumed and the oxygen uptake rate returned to the uninhibited levels.

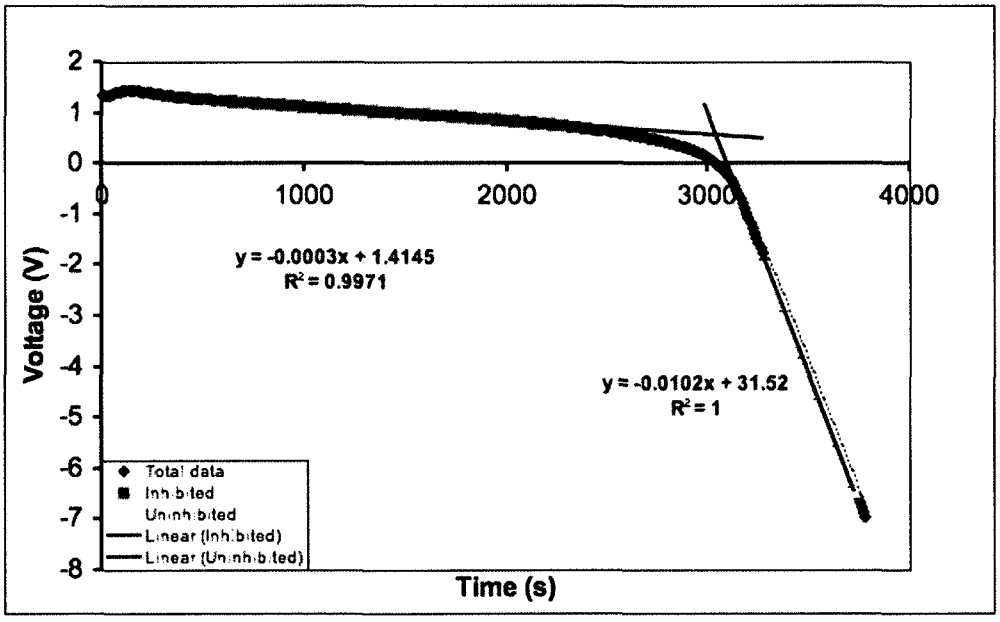

Figure 1.2 Oxygen uptake curve from AIBN-initiated autoxidation of styrene inhibited by ~7 μM PMHC. Inhibition period (τ) is the intersection of the trendlines from inhibited (pink) and uninhibited (yellow) regions.

1.5 Appendix

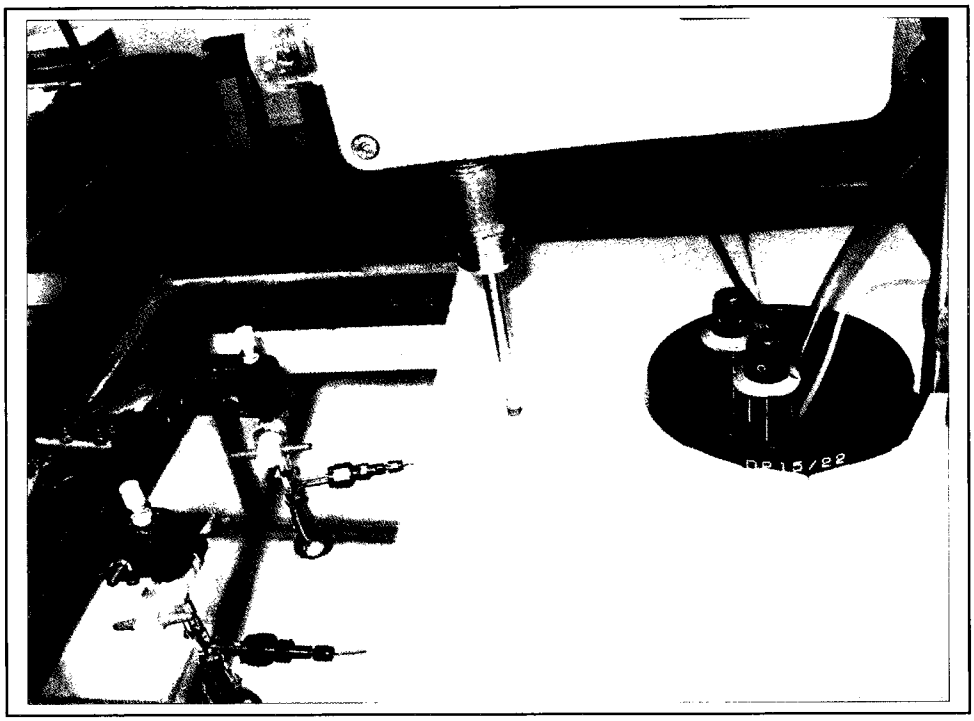

App. Figure 1.1 **Setup of the oxygen uptake apparatus. Notice the cells in the water bath (left) and red/green control knobs (right).**

MOUNT ALLISON UNIVERSITY
SACKVILLE, NEW BRUNSWICK
CANADA
E0A 3C0

DR. L. ROSS C. BARCLAY
CARNEGIE PROFESSOR
OF CHEMISTRY

CHEMISTRY DEPARTMENT
PHONE (506) ~~536-2040, EXT. 478~~
364-2369

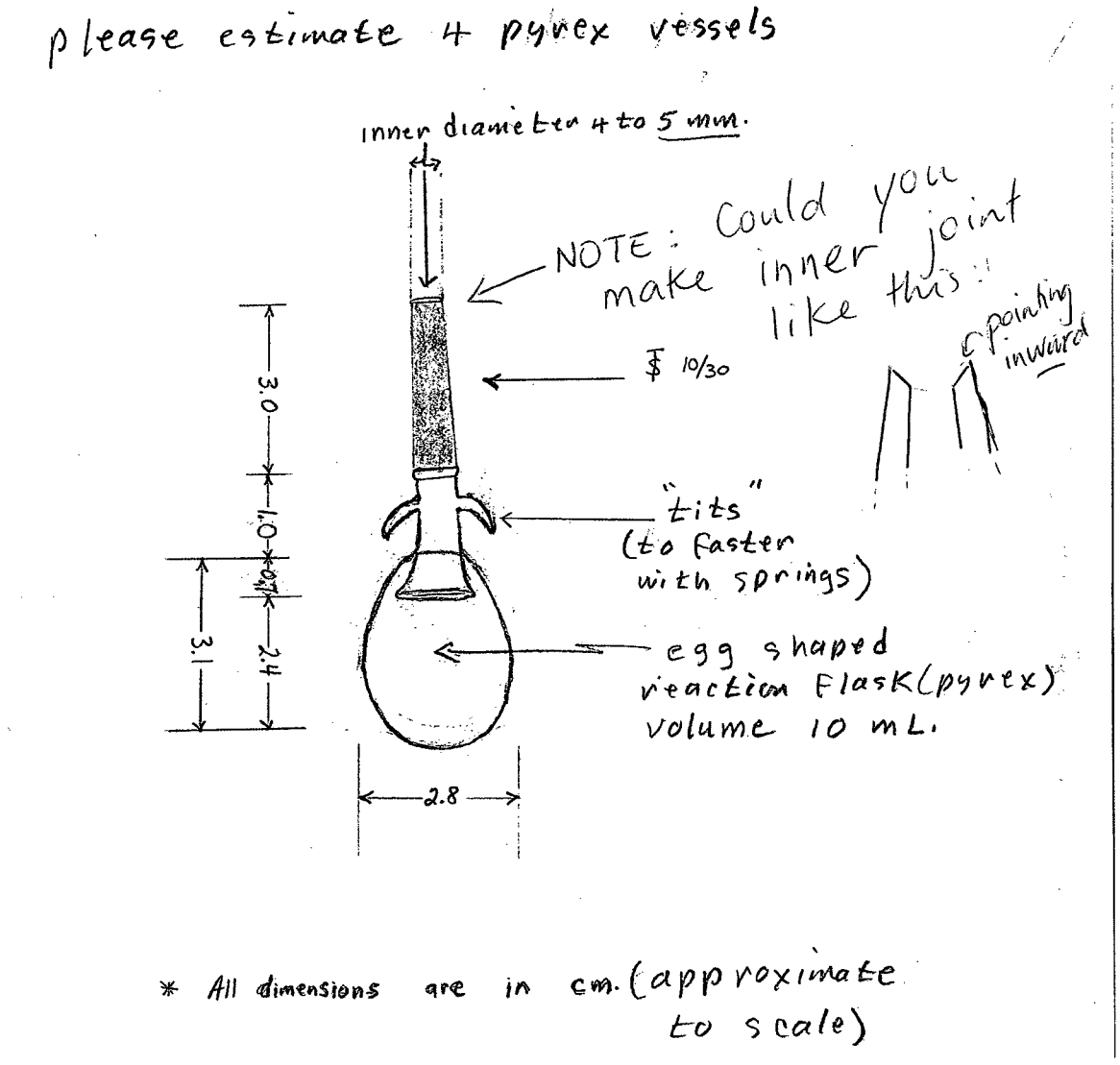

App. Figure 1.2 Cells designed for the oxygen uptake experiments (drawing received from Ross Barclay, Mount Allison University, N.B.)

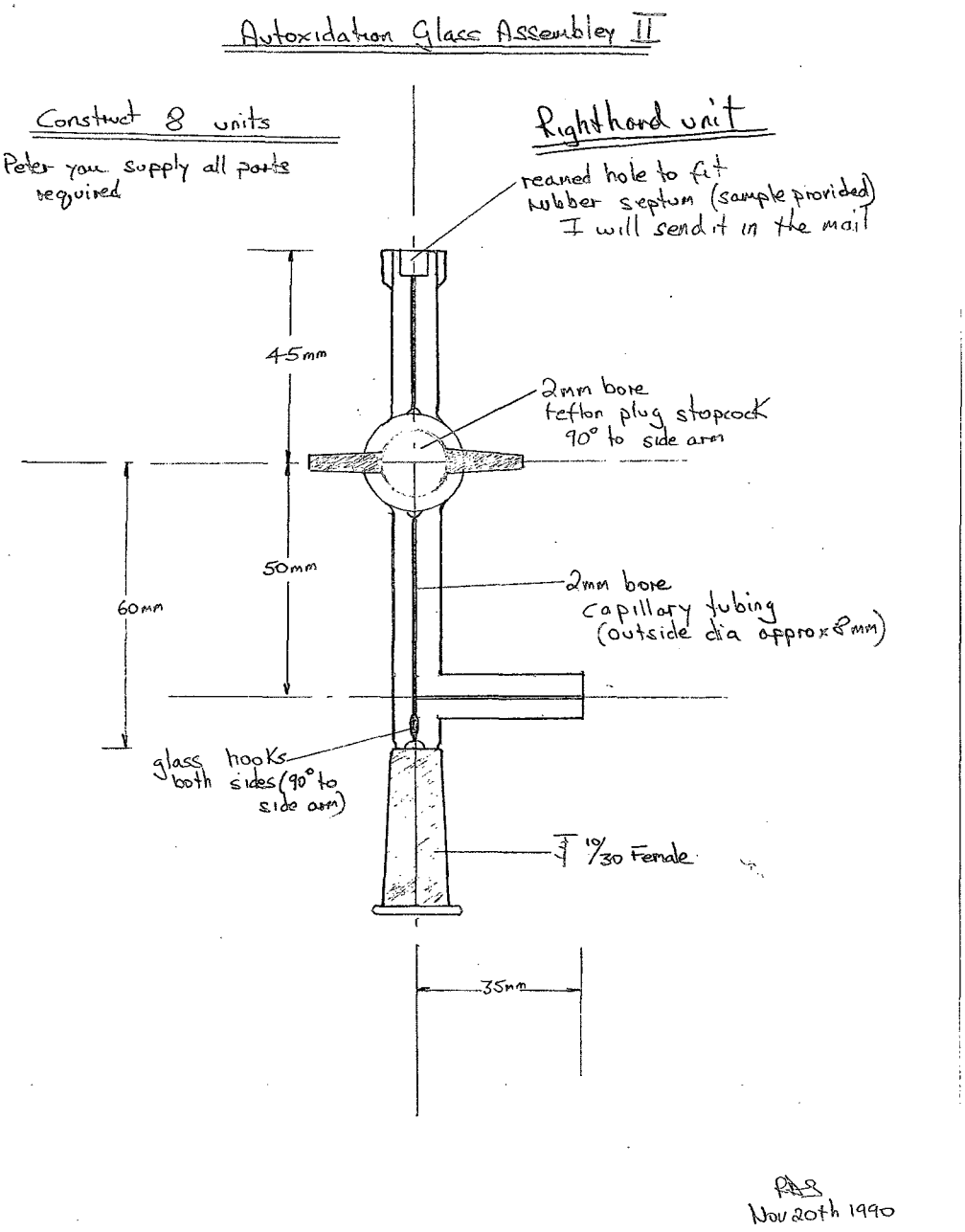

App. Figure 1.3 ***Diagram of segment of oxygen uptake apparatus to which the cells are attached, and through which sample injections are performed. Note that the glass capillary leading to the right is attached to hollow springs that lead to the pressure transducer compartment. (drawing received from Ross Barclay, Mount Allison University, N.B.)***

1.6 References

(1) Solomons, G.; Fryhle, C. *Organic Chemistry (7th ed.)*; John Wiley and Sons Inc.: New York, 2002.

(2) Turro, N. J. *Modern Molecular Photochemistry*; University Science Books: Sausalito, California, 1991.

(3) Fox, M. A.; Whitesell, J. K. *Organic Chemistry (3rd ed.)*; Jones and Bartlett Publishers: Sudbury, Massachusetts, 2004.

(4) Howard, J. A.; Ingold, K. U. *Can. J. Chem.* **1965**, *43*, 2729-2736.

(5) Van Hook, J.; Tobolsky, A. *J. Am. Chem. Soc.* **1958**.

(6) Vinquist, M.; Barclay, R., Notes for the use of Pressure Transducer, Mount Allison University.

(7) OOI Sensors. Fiber Optic Sensors System. Installation and Operation Manual. Document Number FOXY-AL300-000-02-0207. 2007.

2 Solvent-Independent Antioxidant Activity of HP-136 Dimer

2.1 Autoxidation Process

Degradation of various materials, including biological systems, is often a result of oxidative damage caused by free radical reactions[1]. Even a small amount of free radicals can lead to widespread harmful effects, since radicals are able to initiate self-propagating chain reactions. The presence of free radicals therefore leads to an amplification of the degradation process. In an oxygen-containing environment, such as air, the propagating chain reaction often involves a step in which O_2 is consumed; this is referred to as an autoxidation[2] (Scheme 2.1).

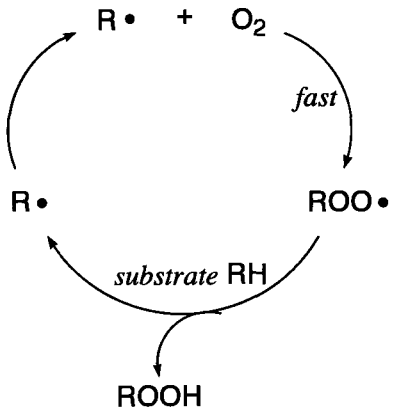

Scheme 2.1 Chain propagation cycle in the autoxidation of substrate (RH)

When a free radical is generated by an initiation reaction – thermal, photochemical, enzymatic, or other – it can react with surrounding molecules. This radical often rapidly reacts with molecular oxygen to form a peroxyl radical. At this point, the peroxyl radical reacts with another surrounding molecule to form a radical

ready for reaction with O_2. The resulting radical continues the propagation cycle. Thus, one molecule of dioxygen is consumed during each propagation cycle as shown in Scheme 2.1.

In the absence of antioxidants, autoxidation termination reactions involve the reaction of two peroxyl radicals leading to non-radical products[1,3]. Note that while this termination *removes* two radicals from the environment, the initiation reaction usually leads to the *formation* of two radicals.

Autoxidations can be retarded by the addition of antioxidants. The antioxidant provides an additional termination pathway for the radicals involved in propagation, thus inhibiting the rate of autoxidation (Scheme 2.2). Reaction with the antioxidant usually leads to radicals that cannot propagate the oxidation chain and, eventually, to non-radical products.

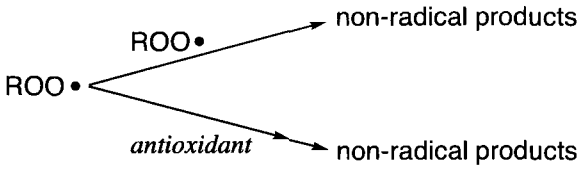

Scheme 2.2 Autoxidation termination pathways

2.2 Common Antioxidants – Mechanism of Phenolic Chain-Breaking Antioxidants

Free radicals and reactive oxygen species (ROS) are constantly being generated in our surroundings. The ROS generally originate from molecular oxygen that has not been fully reduced to water. Most of these species are unstable radicals; superoxide ($O_2^{-}\bullet$), hydroperoxyl (HOO•), peroxyl (ROO•), alkoxyl (RO•), and hydroxyl (HO•). The notable exceptions are singlet oxygen and hydrogen peroxide. The excited form of dioxygen – singlet oxygen ($^1O_2$) – is unstable, but is not a free radical. Hydrogen peroxide (H_2O_2) is also considered an ROS, although "pre-ROS" is a more accurate description – it is a stable compound that can easily generate ROS.

The free radicals and ROS can react with, and damage, various substrates. In a living organism, for example, these "substrates" are biologically vital molecules such as DNA, lipids, and proteins, where alterations can disrupt signaling pathways and ultimately lead to detrimental effects. It should be mentioned that ROS are also a byproduct of normal cell metabolism and play a role in well-functioning cell signaling[4,5]. However, disturbance of this delicate balance, where a large excess of ROS are created, can be harmful. In fact, free radical reactions play an important role in various pathological conditions and have been invoked in the process of ageing. To combat the damaging free radicals and ROS, nature has evolved

antioxidant strategies that convert harmful free radicals into less reactive, benign species.

There are many different types of antioxidants encountered in nature. A large number of them are enzymes found inside the cells. Some, such as transferrin, lactoferrin and ferritin, prevent the formation of radicals and ROS by sequestering iron. Other enzymes convert ROS, mostly superoxide and hydrogen peroxide, into unreactive forms[6-8]. Superoxide dismutase, catalase and glutathione peroxidase are examples of enzymatic antioxidants. If all else fails, the radical reactions must be stopped directly. This can be done by another type of protective molecules called chain-breaking antioxidants. These molecules provide another line of defense against oxidative stress; they inhibit the autoxidation cycle after it has been initiated.

Apart from biological systems, chain-breaking antioxidants are also widely used in industry. They are common additives in creams, food, etc., and are added to various materials, such as plastics, to prevent their degradation due to thermal or photochemical oxidation.

Chain-breaking antioxidants hinder the propagation cycle by reacting with peroxyl radicals to give products that do not participate in the propagation reaction, thus stopping further oxidative damage. This means that, for the inhibition of autoxidation, one of the key characteristics of a chain-breaking antioxidant is their fast reaction with peroxyl radicals. Another important feature of a good antioxidant is its lack of reactivity and the lack of reactivity of its intermediate radicals toward

molecular oxygen. If the antioxidant radical reacted with oxygen, the resulting peroxyl radical would simply continue the autoxidation reaction. Common chain-breaking antioxidants that fit these criteria are phenolic molecules, with α-tocopherol (Vitamin E) being one of the most efficient examples[2] – its rate constant of inhibition, k_{inh}, is approximately 3.2 x 10^6 $M^{-1}s^{-1}$ (Scheme 2.3).

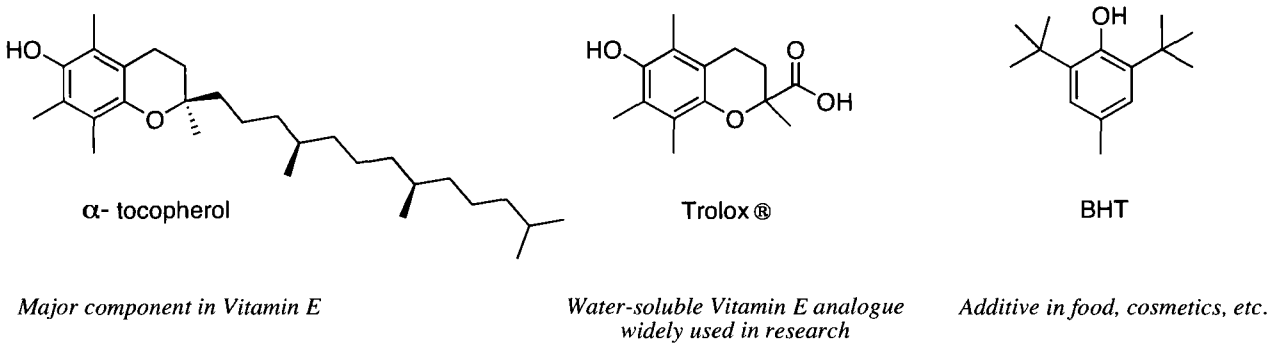

Scheme 2.3 Examples of phenolic chain-breaking antioxidants

These phenolic antioxidants stop peroxyl radicals by transferring a hydrogen atom to generate a phenoxyl radical[2,9] (Equation 2.1):

$$ROO\bullet + Ar\text{-}OH \xrightarrow{k_{inh}} ROOH + \underset{\textit{phenoxyl radical}}{Ar\text{-}O\bullet}$$

$$Ar\text{-}O\bullet + O_2 \not\longrightarrow \text{slow / no reaction}$$

Equation 2.1

Note that the resulting antioxidant-derived phenoxyl radical is rather persistent, and unreactive towards oxygen, in accordance with the required criteria.

If the phenoxyl radical reacted with oxygen, it would simply continue the autoxidation cycle as is the case for some hydroquinone-derived phenoxyl radicals[10]. Ideally, the resulting phenoxyl radical will trap another peroxyl radical. Therefore, a single phenolic antioxidant molecule is able to trap two peroxyl radicals (stoichiometric factor, $n = 2$).

Phenolic antioxidants do have a major disadvantage. Due to the presence of an O-H bond, common phenolic antioxidants tend to be very sensitive to solvent effects. This effect is due to the phenol's ability to interact with the solvent through hydrogen bonding, thus lowering the phenol's hydrogen-atom donating ability (Scheme 2.4). As a result, the antioxidant activity in hydrogen-bond accepting (HBA) solvents dramatically decreases. This phenomenon has been thoroughly investigated by Ingold, Scaiano and others[9,11,12].

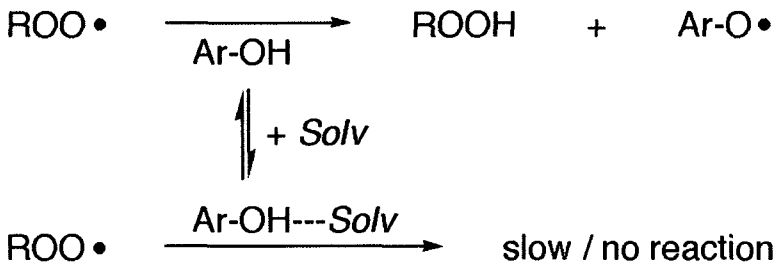

Scheme 2.4 Effect of hydrogen-bond accepting solvents (*Solv*) on common phenolic antioxidant activity.

2.3 Criteria for Reducing Radical Reactivity towards Oxygen

As already mentioned, in order to be a good antioxidant, a molecule must be a good hydrogen donor, while producing a radical that cannot participate in the propagation of autoxidation[13].

Hydrogen donors that yield carbon-centered radicals are rarely good antioxidants since most carbon-centered free radicals react rapidly with oxygen, often at rates approaching diffusion control. The result would be another peroxyl radical that can further propagate the oxidation chain rather than terminate it[14]. For example, 1,4-cyclohexadiene is a poor antioxidant even though it is a good hydrogen atom donor[15].

One of the exceptions is a molecule called Irganox HP-136®, which is a lactone commercialized by CIBA and sold as an antioxidant for industrial applications:

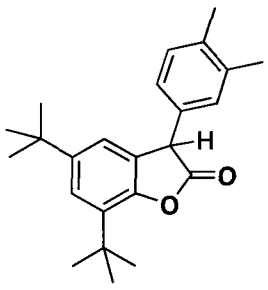

HP-136 monomer

This molecule has long been of research interest in the Scaiano lab. Initially, Scaiano became curious by how such a structure could act as an antioxidant. Results of laser flash photolysis (LFP) studies demonstrated that the HP-136 carbon-centered radical displays highly reduced reactivity towards oxygen[13]. Moreover, the 2-coumaranone backbone was found to be an important structural component for reducing reactivity of lactone-derived radicals. In the case of carbon-centered radicals, "reduced reactivity" refers to no reactivity with oxygen on a 100 μs time scale. These findings were surprising and very interesting because previously, steric hindrance and electron delocalization through resonance were thought to be the major factors contributing to decreased radical reactivity. Through further investigations, and also by analyzing known unreactive carbon-centered radicals, Scaiano and colleagues proposed five criteria that control the reactivity of carbon-centered radicals with molecular oxygen[15]:

i. Benzylic resonance effects

ii. Steric effects

iii. Favourable stereoelectronic effects

iv. Unpaired spin delocalization on heteroatoms

v. Electron withdrawing effects

Note that these criteria are in no specific order of importance – certain factors may be essential in one molecule, but insignificant in another. Some examples of carbon-centered radicals unreactive towards oxygen are shown in Scheme 2.5.

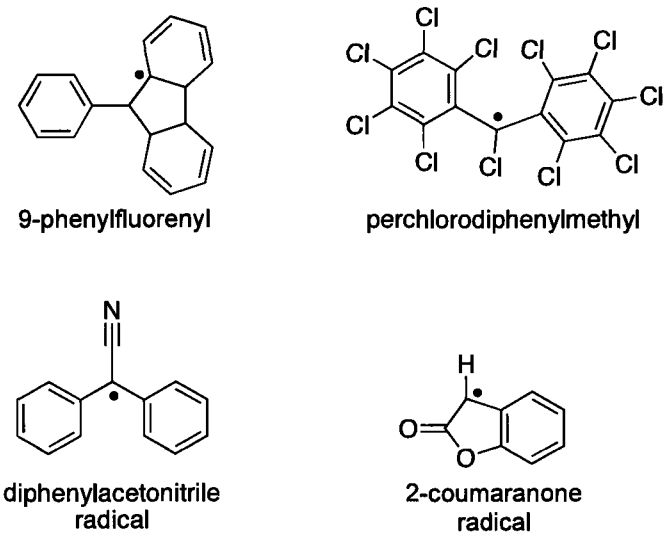

9-phenylfluorenyl | perchlorodiphenylmethyl

diphenylacetonitrile radical | 2-coumaranone radical

Scheme 2.5 Examples of carbon-centered radicals with reduced reactivity towards molecular oxygen.

Radicals become more stable if electrons are delocalized on aromatic rings by resonance. The 9-phenylfluorenyl molecule, which has reduced reactivity to oxygen, is one example where this effect plays a large role in radical stabilization[15]. Bulky substituents that hinder access to the radical site could also contribute to radical stabilization, as is the case for perchlorodiphenylmethyl and some related compounds described by Ballester[16]. As Scaiano and co-workers showed, some carbon-centered radicals with rather simple structures, where steric effects are not significant, also have reduced reactivity towards oxygen[15]. In the case of 2-

coumaranone and its derivatives, for example, the presence of a lactone ring leads to forced planarity and better electron delocalization. Importantly, this achieves spin delocalization on oxygen, which provides some oxygen-centered radical character and also contributes to stabilization. Finally, electron withdrawing effects can also influence radical reactivity towards oxygen. When electron withdrawing groups are added to a molecule, the radical site becomes more electrophilic, and therefore less reactive towards molecular oxygen, which is also electrophilic. For example, diphenylmethyl radical reacts rapidly with oxygen, but diphenylacetonitrile radical shows reduced reactivity[17].

In the HP-136 radical, all of the five criteria are present, explaining why this radical is especially unreactive towards oxygen.

2.4 Radically Different Antioxidant Dimers

When I arrived in the Scaiano group, I began working with the HP-136 dimer. Not long before I joined the group, a fellow graduate student, Mathieu Frenette (Ph.D. 2008), synthesized and characterized the HP-136 dimer, as well as other similar dimers[17]. He discovered that these dimer molecules show antioxidant activity. The actual antioxidants in this system are the carbon-centered HP-136 radicals. As discussed previously, these radicals have highly reduced reactivity with oxygen (Scheme 2.6, reaction 2), and for this reason they instead prefer to react with each other to form head-to-head dimers held together by atypically weak carbon-carbon bonds. These radicals do, however, react quickly with peroxyl radicals (Scheme 2.6, reaction 3). The discovery of compounds where carbon-centered radicals are the active antioxidant species constitute a new class of antioxidants we call "Radically Different Antioxidants".

In solution, these dimers are present in thermal equilibrium with their radicals, and under usual experimental conditions this equilibrium strongly favours the dimer form – more than 99% of the compound is in its dimer form[18] (Scheme 2.6, reaction 1). However, if the dimer concentration is increased, a higher percentage of the radical form would be expected due to the equilibrium shift according to Le Chatelier's principle. The bond dissociation energies (BDE) of the dimers of these systems have been found to lie between 23 and 26 kcal/mol[17]. These bonds are much weaker when compared to typical C-C BDE values of ~83 kcal/mol[19]. While

the dimers have weak C-C bonds, we describe them as having "dynamic stability" through constant dissociation to the carbon-centered radicals, and re-association of the latter, in remarkably well-behaved equilibria[17].

The goal of my work was to study the antioxidant properties of one of these carbon-centered radical dimers. The HP-136 dimer was chosen because, in addition to being a commercially important compound, it was the best behaved from

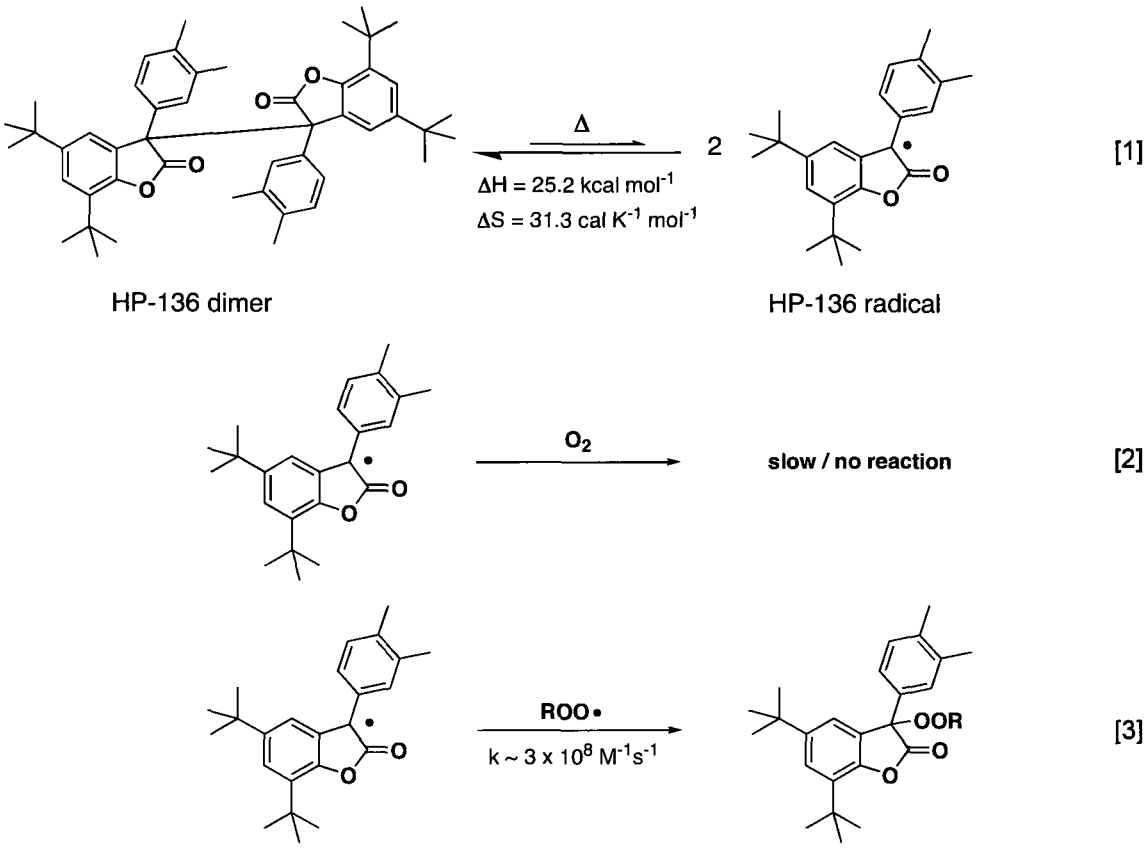

Scheme 2.6 Dynamic stability of HP-136 dimer in solution [1], and reactivities of the HP-136 radical with dioxygen [2] and peroxyl radicals [3]. Previously reported thermodynamic properties and rate constant are shown[20].

the other structurally related dimers. In particular, I studied the effect of solvent on antioxidant activity of HP-136 dimer. In contrast to common phenolic antioxidants that exhibit strongly solvent-dependent antioxidant activity, the HP-136 radical cannot hydrogen bond at its reactive site and is thus expected to exhibit little or no solvent-dependence on its antioxidant activity.

To test this idea, the antioxidant activity of HP-136 dimer was measured in a range of solvents that have a variety of hydrogen-bond acceptor (HBA) activities, using the Inhibited Oxygen Uptake method[21-23] (*vide infra*). The solvents were chosen according to a β_2^H scale that was developed by Abraham and colleagues[24]. The scale is based on log(K) values for hydrogen bond complexation of a series of bases against a number of reference acids, and covers a range of 0.00 to 1.00, where non-HBA solvents such as alkanes are given 0.00, and a very strong H-bond acceptor, hydromethylphosphoric triamide (HMPA), is given 1.00. This scale was determined for bases in dilute solutions, but it is also widely used in the literature for comparison of solvent basicity[9,10] – the scale in bulk solutions is in most cases very similar to that of dilute solutions[25], but it is important to keep in mind that it may be different in some cases. Nevertheless, the β_2^H scale is the most extensive hydrogen-bond basicity scale available, and is suitable for relative solvent effect determination.

Chain-breaking antioxidants whose activity is also solvent-independent would address a major problem with regards to standard phenolic antioxidants. They may

have a significant advantage over common phenolic antioxidants in industrial applications involving polar environments where phenolic antioxidants are the least effective[9].

2.5 Inhibited Oxygen Uptake Method

The Inhibited Oxygen Uptake (IOU) method is the most direct technique for assessing the antioxidant activity of a compound, since it directly measures the amount of oxygen consumed during autoxidation reactions. In this work, the IOU method was used to determine the antioxidant activity of HP-136 dimer, as well as to test the effect of solvents on its performance as an antioxidant. The effect of solvent on the antioxidant activity of a representative phenolic antioxidant, 4-methoxyphenol, was also measured for comparison.

The experiment is similar to the cell calibration experiment discussed in the Introduction (Chapter 1). The idea is to set up an autoxidation reaction in the sample cell, while the reference cell contains all the same ingredients, minus the radical initiator, to ensure identical pressure between the cells prior to initiation. The system in these experiments once again uses styrene as the autoxidizable substrate (Scheme 2.8). Note that the product of styrene oxidation is a co-polymer of styrene and dioxygen. However, there are several important distinctions – in these experiments, we are using a mixture of solvent and styrene substrate, instead of pure styrene. We are also comparing two antioxidants – 4-methoxyphenol and HP-136 dimer, and are using PMHC (2,2,5,7,8-pentamethyl-6-hydroxychroman) for stoichiometric factor determination (Scheme 2.7).

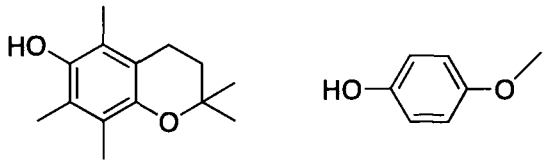

PMHC 4-methoxyphenol

Scheme 2.7 The phenolic antioxidants used in our experiments.

In the experiments, a mixture of solvent and ~2.6 M styrene is first equilibrated overnight at 30°C. The autoxidation begins once a radical azo-initiator (AIBN or V-601, depending on solubility) is injected only into the sample cell to a final concentration of ~18 mM (see Experimental section for further details).

The uninhibited autoxidation reaction is recorded by measuring the rate of oxygen uptake. Next, an antioxidant is injected, resulting in inhibition of the autoxidation, thus the observed rate of oxygen uptake decreases. This inhibition period continues until all of the antioxidant is consumed, at which point the autoxidation rate returns to the uninhibited levels. The inhibition period (τ), defined as the time necessary to consume the antioxidant, is estimated from the intercept of inhibited and uninhibited rates of oxygen uptake in the resulting oxygen uptake curves, similar to that described in section 1.4.8 (Figure 1.2).

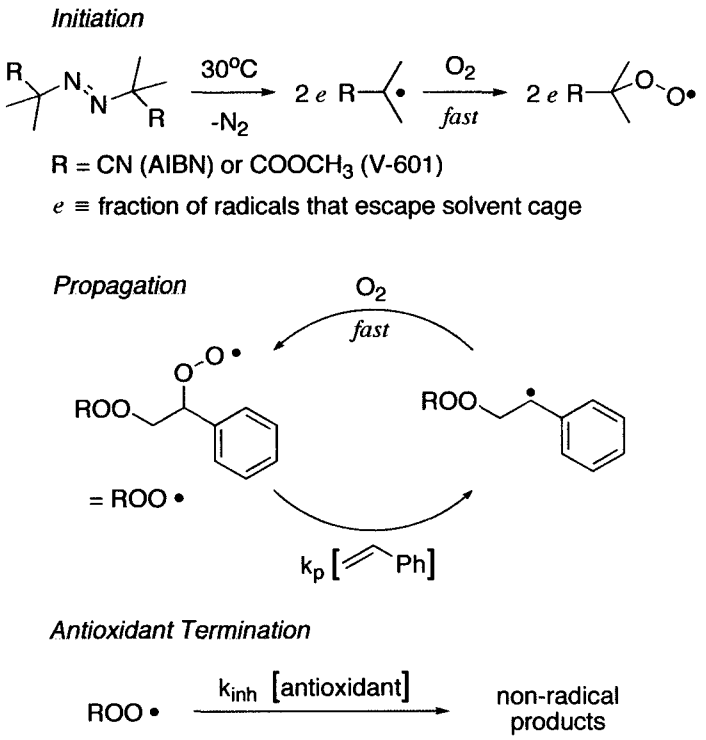

Scheme 2.8 Autoxidation system used in our experiments. Note that the length of "R" grows by one "monomer + O_2" unit during each cycle.

The kinetic parameter representing the antioxidant activity of a compound is the rate constant of inhibition, k_{inh} (Scheme 2.8), which describes how efficiently the compound can react with and trap peroxyl radicals. The oxygen uptake curves allow us to estimate k_{inh} using the rate expression in equation (5), and its integrated form, equation (6):

$$\left\{\frac{d[O_2]}{dt}\right\}_{inh} = -\frac{k_p[RH]R_i}{nk_{inh}[AH]} \qquad (5)$$

$$\Delta[O_2]_t = -\frac{k_p}{k_{inh}}[RH]\ln(1 - t/\tau) \qquad (6)$$

where *t* is time; [RH] is the concentration of the substrate, styrene; R_i is the rate of initiation of autoxidation; *n* is the stoichiometric factor; [AH] is the concentration of antioxidant; k_p is the propagation rate constant (41 $M^{-1}s^{-1}$ for styrene[26] at 30 °C); and τ is the inhibition period. From equation (6), a plot of $\Delta[O_2]$ vs $-\ln(1 - t/\tau)$ gives a straight line with the slope $(k_p/k_{inh})[RH]$, from which k_{inh} can be calculated, provided a substrate with a known k_p is used, such as styrene.

However, the IOU method for measuring k_{inh} requires that there be a significant number of propagation cycles during the inhibition period, so that there is a measurable competition between the propagation and inhibition reactions. The parameter for checking the number of propagation cycles is chain length, since during each propagation cycle one styrene molecule is added to the chain. Chain length, *v*, is defined as the rate of propagation (or, the rate of O_2 uptake) divided by the rate of initiation, as shown in equation (7):

$$v = \{-d[O_2]/dt\}_{inh} / R_i \qquad (7)$$

$$R_i = \frac{n[PMHC]}{\tau} \qquad (8)$$

A chain length > 4 is considered sufficient for k_{inh} determination using the IOU method. Recall from Chapter 1 that PMHC is a Vitamin E analogue that is also known to trap two peroxyl radicals, *i.e.*, *n* = 2. However, in the weaker HBA solvents PMHC is too strong an antioxidant to reliably measure k_{inh} (i.e., chain length is often < 4). For this reason, a weaker antioxidant, 4-methoxyphenol, whose k_{inh} values

could be measured more reliably, was employed for comparative purposes (Scheme 2.7). PMHC was, however, required to determine the rate of initiation of autoxidation, R_i, and to calculate stoichiometric factors, *n*, using equation (8).

2.6 Results and Discussion

We measured the oxygen uptake kinetics for the autoxidation of styrene in solvents of varying polarity to study the solvent effect on three antioxidants' performance. The goal was to demonstrate minor solvent effects on the antioxidant activity for a representative "radically different antioxidant", HP-136 dimer, and compare this to the dramatic solvent effects expected for a typical phenolic antioxidant, 4-methoxyphenol. In each system, we also measured the oxygen inhibition due to PMHC, an effective and well-behaved antioxidant based on the structure of Vitamin E's main component. The oxygen uptake data are presented in Figure 2.1 with the uninhibited oxygen uptake curve (no antioxidant) and with PMHC, 4-methoxyphenol, or HP-136 dimer acting as the chain-breaking antioxidant.

The analysis of the oxygen uptake data is done, when possible, using the integrated oxygen uptake kinetics according to equation (6). According to this equation, a plot of $\Delta[O_2]$ vs $-\ln(1-t/\tau)$ should yield a slope equal to $k_p[RH]/k_{inh}$, and this data is shown for HP-136 dimer in different solvents (section 2.6.1).

The tabulated results are presented in Table 2.1 – the treatment of the oxygen uptake data to obtain inhibition rate constants is described in section 2.6.1. A graph summarizing the results is displayed in Figure 2.2.

See figure caption on the next page.

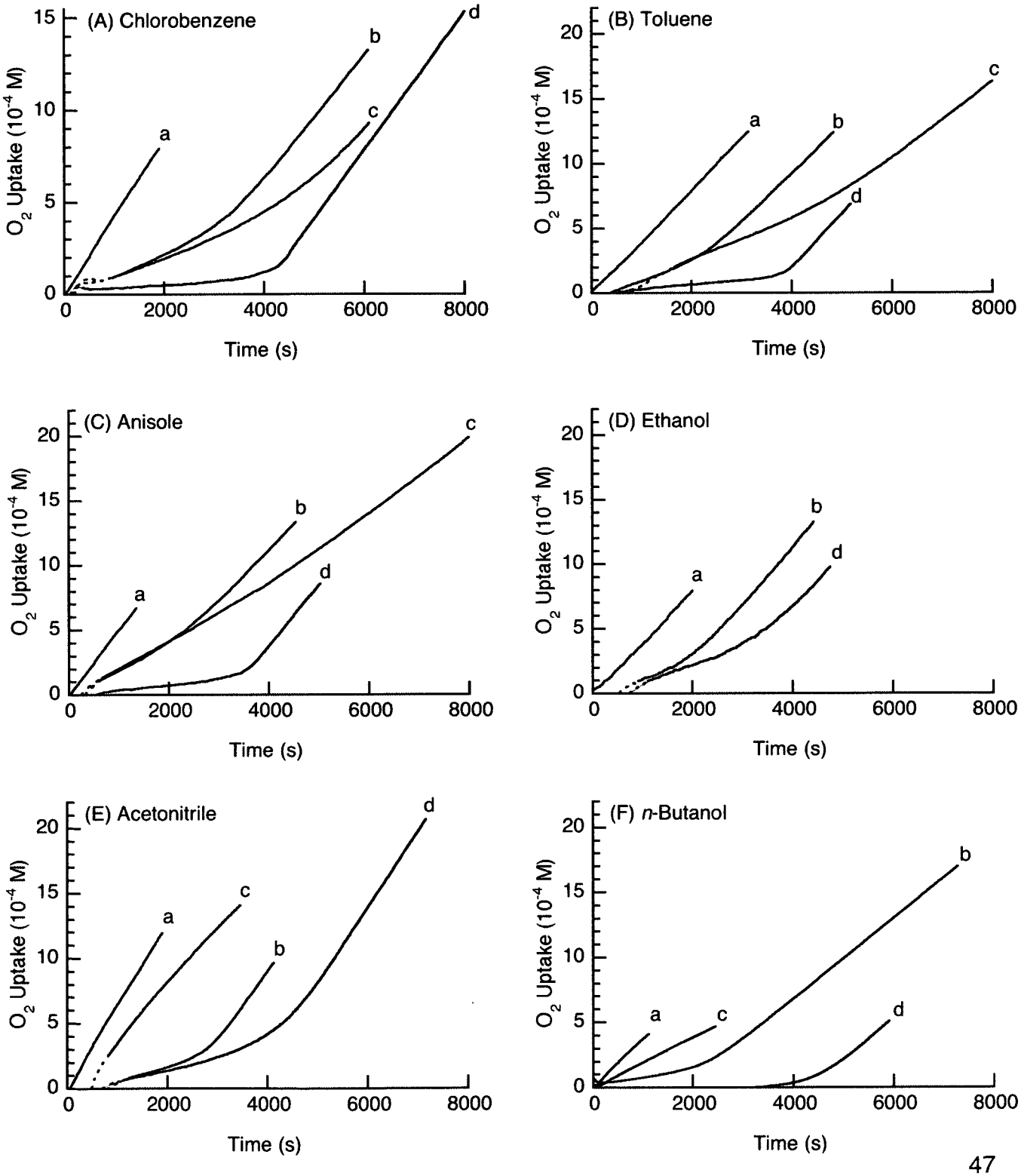

Figure 2.1 (previous page) Representative oxygen uptake curves for the different solvents tested. Autoxidation of styrene, ~2.6 M, in (A) chlorobenzene, (B) toluene, (C) anisole, (D) ethanol, (E) acetonitrile and (F) *n*-butanol , initiated with AIBN or V-601, ~18 mM, at 30°C. Curve a: uninhibited oxygen uptake. Curve b: inhibited by HP-136 dimer, ~4.6, 7.7, or 9.1 μM. Curve c: inhibited by 4-methoxyphenol, ~4.6 μM in toluene, anisole and chlorobenzene; ~13 μM in acetonitrile; ~18 μM in butanol. Curve d: inhibited by PMHC, ~4.6 μM. Dashed lines indicate equilibration period of the system.

As hypothesized, the HP-136 dimer exhibits little to no solvent effect on its antioxidant activity, whereas 4-methoxyphenol shows a large solvent effect. With increasing HBA activity of the solvent, the k_{inh} values for 4-methoxyphenol decrease markedly, while the antioxidant activity of the HP-136 dimer are almost invariant, indicating that the antioxidant activity of the HP-136 dimer is not reduced with variations in the HBA activity of the solvent.

Table 2.1 Solvent Effects on Kinetic Data for Inhibition of Styrene Autoxidation at 30°C.

		HP-136 dimer		4-methoxyphenol		PMHC
solvent	**β_2^H**	**n**	**k_{inh} (10^4 $M^{-1}s^{-1}$)**	**n**	**k_{inh}[a] (10^4 $M^{-1}s^{-1}$)**	**k_{inh} (10^4 $M^{-1}s^{-1}$)**
chlorobenzene	0.09	0.89	61 ± 10	2.27	37 ± 10	289 ± 39
toluene	0.14	1.20	75 ± 28	2.65	33 ± 2	225 ± 50
anisole	0.26	1.47	45 ± 10	3.10	13.1 ± 0.8	174 ± 1
ethanol	0.44	1.18	73 ± 21	n/a	(4.8)[b]	50 ± 1
acetonitrile	0.44	0.94	113 ± 39	n/a	1.7 ± 0.3	59 ± 2
n-butanol	0.45	0.89	124 ± 63	n/a	4.7 ± 2.6	121 ± 41

[a] For solvents ethanol, acetonitrile and n-butanol, no clear inhibition period was observed when using 4-methoxyphenol as an antioxidant. Higher antioxidant concentrations and a slightly different kinetic treatment were used to obtain k_{inh}

[b] This rate constant was found to vary from experiment to experiment and should only be regarded as an estimate.

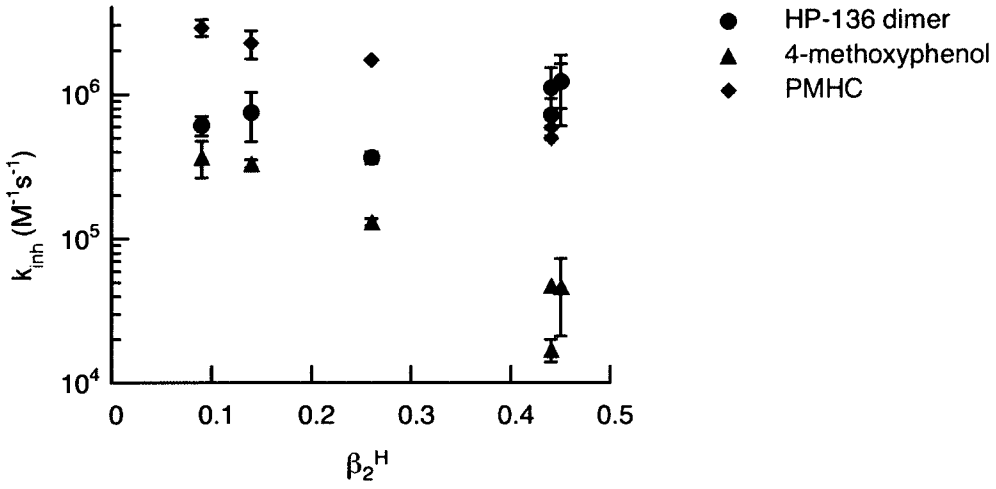

Figure 2.2 Solvent effects on antioxidant activities (k_{inh}) of HP-136 dimer, 4-methoxyphenol and PMHC. Hydrogen-bond accepting abilities of solvents are described by their Abraham factors, β_2^H (chlorobenzene = 0.09, toluene = 0.14, anisole = 0.26, ethanol = 0.44, acetonitrile = 0.44, *n*-butanol = 0.45). Error bars ± 1 standard deviation.

Representative oxygen uptake curves obtained in different solvents are displayed in Figure 2.1. These traces clearly show the difference in solvent effects on the antioxidant behaviour of HP-136 dimer and 4-methoxyphenol. In non-polar, non-HBA solvents, such as chlorobenzene (β_2^H=0.09) and toluene (β_2^H=0.14), both compounds give a well-defined inhibition period, and thus have significant antioxidant activity. However, in stronger HBA solvents, acetonitrile (β_2^H=0.44) and n-butanol (β_2^H=0.45), 4-methoxyphenol shows no well-defined inhibition period although the rate of oxidation is lower than in the absence of any antioxidant. In other words, in acetonitrile and n-butanol 4-methoxyphenol becomes an

autoxidation retarder, rather than an inhibitor. HP-136 dimer, on the other hand, shows a well-defined inhibition period in all solvents.

Another HBA solvent tested was ethanol (β_2^H=0.44). As in the other solvents, the HP-136 dimer showed a well-defined inhibition period. For 4-methoxyphenol, however, the results in this solvent were found to vary from experiment to experiment, and should be regarded as a rough estimate. The irreproducibility is likely a result of the large vapor pressure associated with ethanol. This leads to poor precision in the pressure measurements used to quantify oxygen consumption.

In an intermediate HBA solvent, anisole (β_2^H=0.26), the inhibition period for HP-136 dimer is visible, while for 4-methoxyphenol it becomes more difficult to identify. For some experiments (such as the one shown in Figure 2.1C), its inhibition period could still be obtained, while for others, it was basically a straight line, similar to the acetonitrile and n-butanol traces (data not shown). Thus, 4-methoxyphenol in anisole conveniently illustrates the intermediate nature of solvent effect in an intermediate HBA solvent.

As previously mentioned, PMHC was used to estimate R_i using equation (8), which was then used to calculate the stoichiometric factors of HP-136 dimer and 4-methoxyphenol. Reliable PMHC k_{inh} estimates, however, are difficult to obtain with our system, since PMHC is too good of an antioxidant. In other words, there is insufficient competition between antioxidant termination (k_{inh}[antioxidant]) and autoxidation (k_p[styrene]). Nevertheless, for some traces, the chain length was

satisfactory (ν > 4), and k_{inh} could be estimated for PMHC. These are shown in Figure 2.2, although the results are from only two or three experiments. Small sample sizes also explain the large variability in the errors seen in Table 2.1. As HBA properties of the solvent increase, the PMHC shows a similar trend to 4-methoxyphenol – the solvent reduces the phenolic antioxidants' activity. When comparing the PMHC and HP-136 dimer, the results are very exciting. As previously mentioned, PMHC is a vitamin E analogue, and vitamin E is known to be one of the most efficient chain-breaking antioxidants[2]. It is remarkable that HP-136 dimer, a member of the "radically different" class of antioxidants, is able to match the antioxidant activity of a vitamin E analogue in HBA solvents.

The stoichiometric factor, *n*, is calculated using equation (8) and measured R_i. In all experiments, the stoichiometric factor for the HP-136 dimer in a styrene autoxidation is consistently lower than to the 2.0 expected on the basis of two radicals formed from each dimer molecule. It should be noted that during cumene (isopropylbenzene) autoxidation, *n*=2 for the HP-136 dimer, suggesting that the reduction of stoichiometric factor observed in the styrene system is specific to changing the substrate. Frenette *et al.* suggested a possible explanation for the low stoichiometric factor in styrene[18]. The HP-136 radical could react with the poly(peroxystyrene), which is formed during the autoxidation. In particular, the HP-136 radical could either attack at the peroxide bond or abstract a benzylic hydrogen, generating reactive alkoxyl radicals that would propagate the autoxidation (Scheme 2.9).

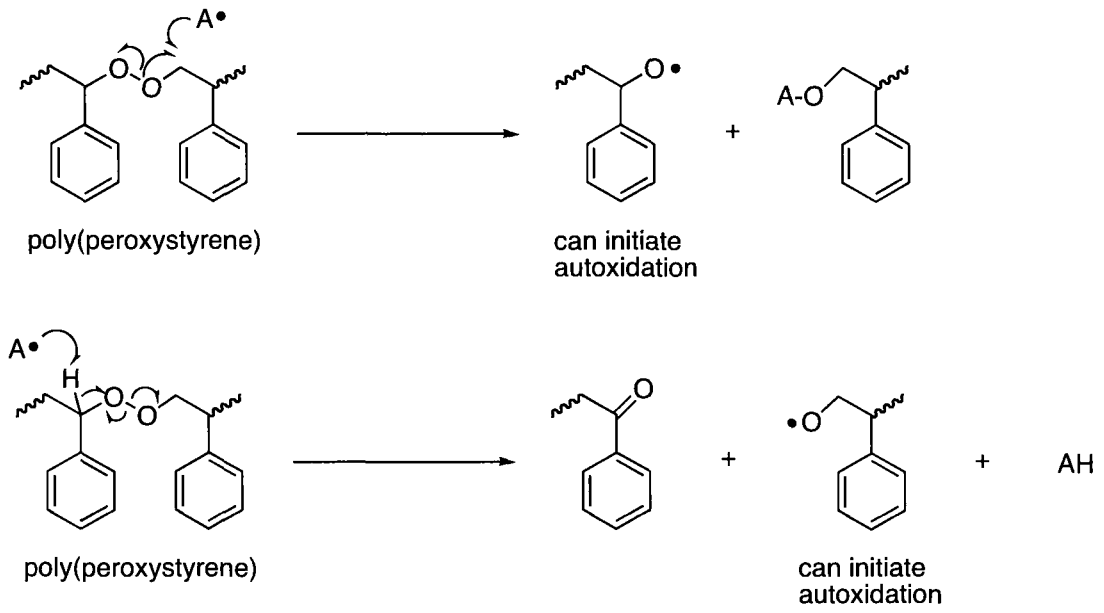

Scheme 2.9 Suggested explanation for n<2 for HP-136 dimer. A• refers to HP-136 radical[18].

In the case of 4-methoxyphenol, values of *n* greater than two are observed, and are likely due to the formation of secondary antioxidants during oxidation of this compound (Scheme 2.10). This can result when peroxyl radicals react at the *ortho* position, although reaction at the *para* position is preferred[1].

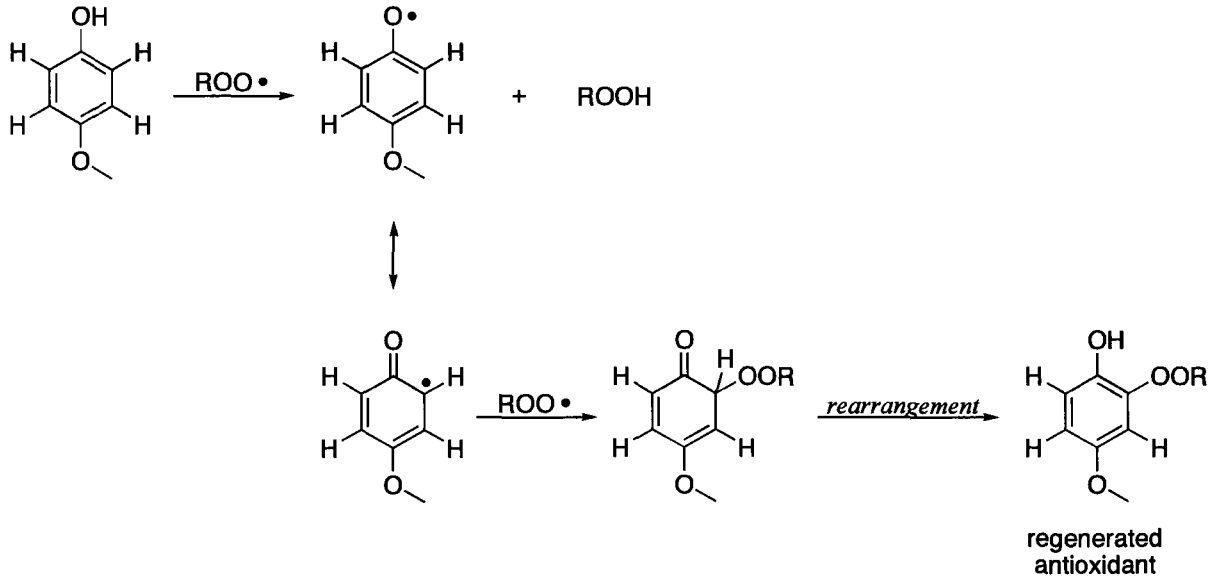

Scheme 2.10 Secondary antioxidant formation from 4-methoxyphenol. Reaction at the *ortho* positions can lead to n>2.

It is interesting to observe that in acetonitrile the inhibition period of HP-136 dimer appears to be, in fact, slightly better defined than in non-HBA solvents, such as chlorobenzene. The obtained k_{inh} is also higher in acetonitrile ($113 \pm 39 \times 10^4$ $M^{-1}s^{-1}$) compared to k_{inh} measured in chlorobenzene ($61 \pm 10 \times 10^4$ $M^{-1}s^{-1}$). An explanation for this increase in antioxidant activity would be a higher degree of dissociation of the HP-136 dimer in acetonitrile. Recall that in solution this dimer is present in a dynamic equilibrium with its radical form (Scheme 2.6, reaction 1). Through UV-visible absorbance studies, it has been estimated that, at 30°C in chlorobenzene, the equilibrium strongly favours the dimer form, and only ~0.08% of the dimer is dissociated into radicals[20]. A similar experiment was conducted in acetonitrile to see if in this solvent the equilibrium behaviour of HP-136 dimer is different, and is more shifted towards the dissociated form. A higher concentration

of the radical form, which is the actual antioxidant, would explain the higher antioxidant activity of HP-136 dimer in acetonitrile. The UV-vis experiments did not detect an increase in dissociation of the HP-136 dimer in acetonitrile compared to chlorobenzene (data not shown).

Other experiments done that involve the HP-136 dimer were ^{1}H-NMR at various temperatures, ranging from +20 to -36°C (data not shown). The preliminary results suggest that compared to room temperature, the HP-136 dimer adapts different conformations at lower temperatures due to slowing down of rotations, however further studies are required.

In conclusion, the HP-136 dimer was found to retain full antioxidant activity in HBA solvents. This valuable property could give the newly-discovered "*radically different antioxidants*" a significant advantage in various industrial applications over traditional phenolic antioxidants that lack this feature.

2.6.1 Kinetic Treatments for k_{inh} Determination

For traces with defined inhibition periods (HP-136 dimer and PMHC), the usual kinetic treatment according to equation [6] was performed. An example of the graph obtained is shown in Figure 2.3.

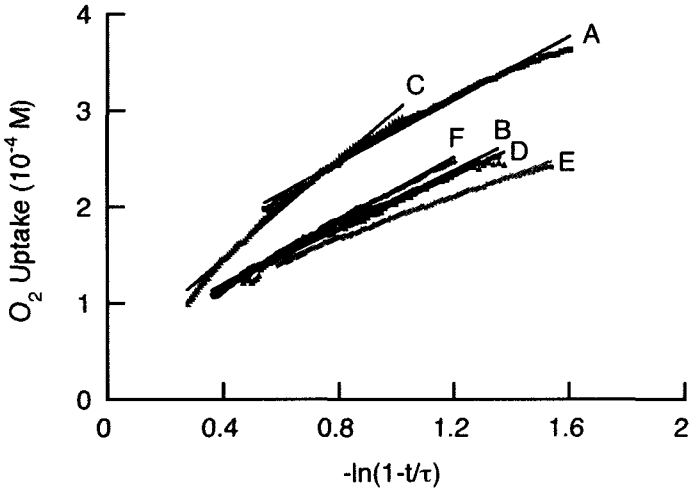

Figure 2.3 Linear fit of HP-136 dimer kinetic data according to equation [6] in (A) chlorobenzene, (B) toluene, (C) anisole, (D) ethanol, (E) acetonitrile and (F) n-butanol.

For the HP-136 dimer, consider that during the inhibition period, most termination reactions are the trapping of peroxyl radicals by HP-136• according to the following mechanism:

$$(\text{HP-136})_2 \underset{K_{eq}}{\overset{\Delta}{\rightleftharpoons}} 2\ \text{HP-136}\bullet \xrightarrow{O_2} \text{no reaction}$$

$$\text{ROO}\bullet + \text{HP-136}\bullet \xrightarrow{fast} \text{non-radical products}$$

In the kinetic treatment of this system, the k_{inh} were derived from the point of view of dimer concentrations (instead of persistent radical concentrations which are subject to uncertainties). Therefore the formal termination rate equation is derived for the more practical reaction shown below:

$$n\ \text{ROO}\bullet + (\text{HP-136})_2 \xrightarrow{k_{inh}} \text{non-radical products}$$

where k_{inh} is the apparent inhibition rate constant and n is the number of peroxyl radicals trapped per dimer. This approach allows us to compare the obtained rate constants with those of typical phenolic antioxidants. It should be noted, however, that the radical concentration is not directly proportional with the dimer concentration, but has the relationship:

$$[HP-136\bullet] = (K_{eq}[HP-136\ dimer])^{1/2} \qquad (9)$$

For this reason, the apparent k_{inh} will increase at lower dimer concentrations and decrease at higher concentrations. This effect is visible in Figure 2.3, where the

linear fits are done on downward curving traces. For consistency, we tried to keep the concentration of the dimer antioxidant approximately constant in each solvent.

A different kinetic treatment was required for experiments where no clear inhibition period is obtained. Such was the case for 4-methoxyphenol in more polar solvents (acetonitrile, n-butanol and ethanol). To determine k_{inh} in these solvents, the differential rate expression (equation (5b)) could be used, since all parameters are known, except k_{inh}. The 4-methoxyphenol concentrations used in this case were higher than in the experiments with defined inhibition periods, because 4-methoxyphenol now acts as an autoxidation retarder, rather than an antioxidant. High concentrations are required to ensure a constant rate of oxygen uptake that has been reduced due to the presence of the retarder.

$$\left\{\frac{d[O_2]}{dt}\right\}_{inh} = -\frac{k_p[styrene]R_i}{nk_{inh}[4-methoxyphenol]} \qquad (5b)$$

In this kinetic treatment we are still assuming, as is done in the usual treatment, that the majority of termination steps occur via reaction of a peroxyl radical and the antioxidant (retarder). This treatment will overestimate k_{inh} as it assumes all termination steps occur by antioxidant and does not account for the peroxyl radical recombination.

2.7 Experimental Details

2.7.1 Materials

Initiator azo-bis(isobutyronitrile), AIBN (Sigma, 98%), was used after re-crystallization from a dichloromethane/n-hexane/ethanol solvent mixture and stored at 4°C. Initiator dimethyl 2,2-azobis(isobutyrate), V-601 (Wako), was stored at 4°C and used as received. CIBA Irganox HP-136® (HP-136 monomer) was a gift from CIBA and used as received. Antioxidant 2,2,5,7,8-pentamethyl-6-chromanol, PMHC (Sigma, 97%), was used after further purification by re-crystallization from n-hexane/dichloromethane. 4-methoxyphenol (Sigma, 99%) was used as received. Styrene (Sigma, 99%) was distilled to remove stabilizers by bulb-to-bulb vacuum distillation and filtered through a silica column (or aluminum oxide). Solvents chlorobenzene (Sigma, HPLC grade), toluene (Sigma, HPLC grade), acetonitrile (Fisher, HPLC grade) and ethanol, 99%, were used directly. Anisole (Sigma, 99%) and n-butanol (Omnisolv, 99%) were filtered through a silica column prior to use.

2.7.2 HP-136 Dimer Synthesis

A saturated solution of HP-136 monomer (2.22 g, 6.3 mmol) was prepared in approximately 100 mL of 2,2,4-trimethylpentane (Sigma, HPLC grade), and sonicated for ~15 minutes to aid solubilization in a Branson 1210 sonicator. The dimerization was started using ~0.25 eq. of TEMPO radical (0.25 g, 1.6 mmol) (Alfa Aesar, 98%). The reaction was stirred overnight in the dark under slow oxygen

purging through sintered glass. Upon addition of TEMPO radical, the solution changed colour from clear to translucent orange. However, approximately 10 minutes after TEMPO addition, the characteristic orange colour of TEMPO radical disappears, indicating that the reaction is underway. The next morning, the solution is orange once again, indicating completion of reaction, and white crystals of HP-136 dimer are present in the reaction flask. The HP-136 dimer was purified by suction filtration, yielding 1.39 g. For further purification, the product was left overnight under vacuum to sublimate the residual TEMPO radical, and then re-crystallized in acetonitrile/dichloromethane for a final yield of 1.03 g (46 % yield). The ^{1}H and ^{13}C NMR matched those previously reported[17].

2.7.3 Inhibited Oxygen Uptake Experiments

The apparatus was prepared as described in section 1.4: the waterbath was set to 30°C, the apparatus vacuumed down, and equilibrated overnight with a mixture of solvent and ~2.6 M styrene (reference cell = 1.4 mL solvent + 0.6 mL styrene; sample cell = 1.3 mL solvent + 0.6 mL styrene). Stock solutions were prepared according to Table 2.2 on the day of the experiment. Stock A solutions were usually prepared in glass vials, and stock B were made in 10 mL volumetric flasks.

Table 2.2 Preparation of Stock Solutions for IOU Experiments

Compound	Desired Mass (g)	Solvent[a]	Volume of Solvent to Stock A (mL)	Volume of Stock A to Stock B[b] (μL)	Approx. Conc. Stock B	Volume of Stock B Injected (μL)
AIBN	0.0600	C T An Ac B	1	N/A	0.36 M	100[d]
V-601	0.0840	T An E	1	N/A	0.36 M	100[d]
PMHC	0.0343	C T An E Ac B	10	200	0.31 mM	30
HP-136 dimer	0.0446	C[c] T	10	500	0.32 mM	30 or 60
4-MeO-phenol	0.0400	C T An	10	100	0.32 mM	30
	0.0400	E Ac B	10	400	1.30 mM	30

[a] C = chlorobenzene, T = toluene, An = anisole, E = ethanol, Ac = acetonitrile, B = *n*-butanol
[b] To make Stock B, Stock A is diluted to final volume of 10 mL in a volumetric flask
[c] Due to solubility issues, C was used to dissolve HP-136 dimer for experiments in An, E, Ac and B
[d] Inject only into sample cell

The next morning, radical azo-initiator (AIBN or V-601, depending on solubility) was injected only into the sample cell to a final concentration of ~18 mM, using a 100 μL syringe. The resulting uninhibited autoxidation reaction was recorded by measuring the oxygen uptake rate, both by the computer and the chart recorder (5 V/scale). Next, the PMHC control (~4.6 μM) was injected into both the reference and sample cells and recorded in the same way to yield an oxygen uptake curve with a defined inhibition period. After the PMHC was consumed and the oxygen uptake rate returned to the uninhibited level, subsequent injections of other

antioxidants can be done. Usually, the sequence of injections was PMHC, HP-136 dimer (two or three trials), and 4-methoxyphenol. Concentrations injected were ~4.6 μM, ~7.1 μM or ~9.1 μM for HP-136 dimer, and ~4.6 μM, ~13.2 μM, or 18 μM for 4-methoxyphenol, depending on experiment.

2.8 Appendix

App. Table 2.1 Oxygen uptake data for all experiments used in Figure 2.2 for HP-136 dimer (A), 4-methoxyphenol (B) and PMHC (C).

(A)

HP-136 dimer Results Summary

Kp styrene (M s)^ -1 = 41

						HP-136 dimer				
Date	Solvent	β_2^H	Ri (Ms-1)	Ri (x E-09 Ms-1)	Run #	n	Kinh/Kp	Kinh/Kp (x E03)	~Kinh	~Kinh (x E04)
18-Jan-08	chlorobenzene	0.09	2.45E-09	2.45	1	0.73	1.16E+04	11.6	4.77E+05	47.7
18-Jan-08	chlorobenzene	0.09	2.45E-09	2.45	2	0.77	1.81E+04	18.1	7.43E+05	74.3
5-Mar-08	chlorobenzene	0.09	2.21E-09	2.21	1	0.99	1.50E+04	15.0	6.16E+05	61.6
5-Mar-08	chlorobenzene	0.09	2.21E-09	2.21	2	0.78	1.50E+04	15.0	6.15E+05	61.5
3-Apr-08	chlorobenzene	0.09	2.40E-09	2.40	1	1.18	1.52E+04	15.2	6.25E+05	62.5
22-Jul-08	chlorobenzene	0.09	2.10E-09	2.10	1	0.88	1.22E+04	12.2	4.98E+05	49.8
22-Jul-08	chlorobenzene	0.09	2.05E-09	2.05	2	0.88	1.70E+04	17.0	6.95E+05	69.5
1-Apr-08	toluene	0.14	2.15E-09	2.15	1	1.21	1.83E+04	18.3	7.51E+05	75.1
8-Apr-08	toluene	0.14	2.41E-09	2.41	1	1.17	1.71E+04	17.1	7.02E+05	70.2
8-Apr-08	toluene	0.14	2.41E-09	2.41	2	1.20	1.04E+04	10.4	4.27E+05	42.7
8-Apr-08	toluene	0.14	2.41E-09	2.41	3	1.21	2.70E+04	27.0	1.11E+06	110.8
18-Mar-08	anisole	0.26	1.93E-09	1.93	2	1.78	4.59E+04	45.9	1.88E+06	188.1
15-Apr-08	anisole	0.26	2.59E-09	2.59	1	1.31	8.29E+03	8.3	3.40E+05	34.0
15-Apr-08	anisole	0.26	2.59E-09	2.59	2	1.31	9.55E+03	9.6	3.92E+05	39.2
15-Apr-09	anisole	0.26	2.33E-09	2.33	1	1.15	1.41E+04	14.1	5.79E+05	57.9
15-Apr-09	anisole	0.26	2.27E-09	2.27	2	1.01	1.18E+04	11.8	4.83E+05	48.3
4-Mar-08	acetonitrile	0.44	2.28E-09	2.28	1	1.01	3.39E+04	33.9	1.39E+06	139.1
4-Mar-08	acetonitrile	0.44	2.28E-09	2.28	2	0.78	3.04E+04	30.4	1.25E+06	124.5
4-Mar-08	acetonitrile	0.44	2.28E-09	2.28	3	1.00	3.81E+04	38.1	1.56E+06	156.3
11-Mar-08	acetonitrile	0.44	2.20E-09	2.20	1	0.78	2.30E+04	23.0	9.41E+05	94.1
12-Mar-08	acetonitrile	0.44	2.35E-09	2.35	1	0.82	1.69E+04	16.9	6.93E+05	69.3
6-May-08	acetonitrile	0.44	2.27E-09	2.27	1	1.01	4.37E+04	43.7	1.79E+06	179.3
6-May-08	acetonitrile	0.44	2.21E-09	2.21	2	0.99	2.18E+04	21.8	8.94E+05	89.4
25-Jul-08	acetonitrile	0.44	2.33E-09	2.33	1	1.04	1.67E+04	16.7	6.86E+05	68.6
25-Jul-08	acetonitrile	0.44	2.27E-09	2.27	2	1.06	2.23E+04	22.3	9.16E+05	91.6
26-Mar-08	ethanol	0.44	2.71E-09	2.71	1	1.23	1.80E+04	18.0	7.36E+05	73.6
26-Mar-08	ethanol	0.44	2.71E-09	2.71	2	1.25	1.25E+04	12.5	5.12E+05	51.2
29-Apr-08	ethanol	0.44	2.77E-09	2.77	1	1.05	2.28E+04	22.8	9.37E+05	93.7
15-Feb-08	butanol	0.45	1.94E-09	1.94	1	0.79	1.61E+04	16.1	6.59E+05	65.9
21-Feb-08	butanol	0.45	1.91E-09	1.91	1	0.80	2.21E+04	22.1	9.04E+05	90.4
21-Feb-08	butanol	0.45	1.91E-09	1.91	2	0.63	1.49E+04	14.9	6.12E+05	61.2
21-Feb-08	butanol	0.45	1.91E-09	1.91	3	0.54	1.54E+04	15.4	6.33E+05	63.3
17-Mar-09	butanol	0.45	2.1E-09	2.10	1	1.04	3.62E+04	36.2	1.48E+06	148.4
17-Mar-09	butanol	0.45	2.07E-09	2.07	2	0.97	3.55E+04	35.5	1.46E+06	145.6
25-Mar-09	butanol	0.45	2.99E-09	2.99	1	1.19	4.47E+04	44.7	1.83E+06	183.4
25-Mar-09	butanol	0.45	2.95E-09	2.95	2	1.13	5.62E+04	56.2	2.30E+06	230.3

HP-136 dimer

Solvent	b2H	Mean *n*	± St. dev of n	Mean Kinh (x E04)	± St. dev of Kinh	
Chlorobenzene	*0.09*	*0.89*	*0.16*	61.0	9.6	
Toluene	0.14	1.20	0.02	74.7	27.9	
Anisole	0.26	1.20	0.14	44.8	10.5	removed outlier
Acetonitrile	0.44	0.94	0.12	112.5	39.3	
Ethanol	0.44	1.18	0.11	72.8	21.2	
n-Butanol	0.45	0.89	0.23	123.6	63.2	

(B)

4-Methoxyphenol Results Summary

Kp styrene (M s)^ -1 = 41

Date	Solvent	β_2^H	Ri (Ms-1)	Ri (x E-09 Ms-1)	Run #	4-Methoxyphenol n	4-Methoxyphenol Kinh/Kp	4-Methoxyphenol Kinh/Kp (x E03)	4-Methoxyphenol ~Kinh	4-Methoxyphenol ~Kinh (x E04)
5-Mar-08	chlorobenzene	0.09	2.21222E-09	2.21	3	2.11	1.19E+04	**11.92**	**4.89E+05**	**48.88**
3-Apr-08	chlorobenzene	0.09	2.40E-09	2.40	2	2.48	7.30E+03	**7.30**	**2.99E+05**	**29.92**
22-Jul-08	chlorobenzene	0.09	2.02E-09	2.02	3	2.22	7.73E+03	**7.73**	**3.17E+05**	**31.68**
1-Apr-08	toluene	0.14	2.15287E-09	2.15	2	2.78	7.73E+03	**7.73**	**3.17E+05**	**31.70**
8-Apr-08	toluene	0.14	2.41274E-09	2.41	4	2.51	8.46E+03	**8.46**	**3.47E+05**	**34.69**
18-Mar-08	anisole	0.26	1.92734E-09	1.93	1	-	3.04E+03	**3.04**	**1.25E+05**	**12.48**
15-Apr-08	anisole	0.26	2.59174E-09	2.59	3	3.10	3.33E+03	**3.33**	**1.36E+05**	**13.65**
15-Apr-09	anisole	0.26	2.23558E-09	2.24	3	1.65	8.57E+03	**8.57**	**3.51E+05**	**35.13**
11-Mar-08	acetonitrile	0.44	2.20E-09	2.20	2	-	5.49E+02	**0.55**	**2.25E+04**	**2.25**
11-Mar-08	acetonitrile	0.44	2.20E-09	2.20	3	-	4.38E+02	**0.44**	**1.80E+04**	**1.80**
12-Mar-08	acetonitrile	0.44	2.34901E-09	2.35	2	-	3.61E+02	**0.36**	**1.48E+04**	**1.48**
6-May-08	acetonitrile	0.44	2.15247E-09	2.15	3	-	3.80E+02	**0.38**	**1.56E+04**	**1.56**
25-Jul-08	acetonitrile	0.44	2.22264E-09	2.22	3	-	3.39E+02	**0.34**	**1.39E+04**	**1.39**
26-Mar-08	ethanol	0.44	2.70877E-09	2.71	3	-	1.18E+03	**1.18**	**4.83E+04**	**4.83**
17-Mar-09	butanol	0.45	2.03696E-09	2.04	3	-	7.18E+02	**0.72**	**2.94E+04**	**2.94**
25-Mar-09	butanol	0.45	2.90468E-09	2.90	3	-	1.60E+03	**1.60**	**6.56E+04**	**6.56**

4-methoxyphenol

Solvent	b2H	Mean *n*	± St. dev of n	Mean Kinh (x E04)	± St. dev of Kinh	
Chlorobenzene	0.09	2.27	0.19	36.8	10.5	
Toluene	0.14	2.65	0.19	33.2	2.1	
Anisole	0.26	3.10	n/a	13.1	0.8	removed outlier
Acetonitrile	0.44	n/a	n/a	1.7	0.3	
Ethanol	0.44	n/a	n/a	4.8	n/a	
n-Butanol	0.45	n/a	n/a	4.7	2.6	

(C)

PMHC Results Summary

Kp styrene (M s)^ -1 = 41

Date	Solvent	Initiator	β_2^H	~Kinh	~Kinh (x E04)
5-Mar-08	chlorobenzene	AIBN	0.09	**3.26E+06**	**326.0**
3-Apr-08	chlorobenzene	AIBN	0.09	**2.94E+06**	**294.0**
22-Jul-08	chlorobenzene	AIBN	0.09	**2.48E+06**	**248.0**
1-Apr-08	toluene	AIBN	0.14	**2.60E+06**	**260.0**
8-Apr-08	toluene	V-601	0.14	**1.90E+06**	**190.0**
18-Mar-08	anisole	AIBN	0.26	**1.73E+06**	**173.0**
15-Apr-08	anisole	V-601	0.26	**1.75E+06**	**175.0**
15-Apr-09	anisole	V-601	0.26	**2.03E+06**	**203.0**
11-Mar-08	acetonitrile	AIBN	0.44	**6.01E+05**	**60.1**
25-Jul-08	acetonitrile	AIBN	0.44	**5.79E+05**	**57.9**
26-Mar-08	ethanol	V-601	0.44	**4.92E+05**	**49.2**
29-Apr-08	ethanol	V-601	0.44	**5.04E+05**	**50.4**
15-Feb-08	butanol	AIBN	0.45	**7.59E+05**	**75.9**
25-Mar-09	butanol	AIBN	0.45	**1.31E+06**	**131.0**
25-Mar-09	butanol	AIBN	0.45	**1.56E+06**	**156.0**
21-Feb-08	butanol	AIBN	0.45	**n/a**	**n/a**
17-Mar-09	butanol	AIBN	0.45	**n/a**	**n/a**

Solvent	b2H	Mean Kinh (x E04)	± St. dev of Kinh
Chlorobenzene	0.09	289.3	39.2
Toluene	0.14	225.0	49.5
Anisole	0.26	183.7	16.8
Acetonitrile	0.44	59.0	1.6
Ethanol	0.44	49.8	0.8
n-Butanol	0.45	121.0	41.0

2.9 References

(1) Ingold, K. U. *Acc. Chem. Res.* **1969**, *2*, 1-9.

(2) Burton, G.; Doba, T.; Gabe, E.; Hughes, L.; Lee, F.; Prasad, L.; Ingold, K. U. *J. Am. Chem. Soc.* **1985**, *107*, 7053-7065.

(3) Denisov, E. T.; Denisova, T. G. *Handbook of Antioxidants*; 2nd ed.; CRC Press: Boca Raton, 2000.

(4) D'Autreaux, B.; Toledano, M. *Nat. Rev. Molec. Cell Biol.* **2007**, *8*, 813-824.

(5) Cash, T.; Pan, Y.; Simon, M. *Free Rad. Biol. Med.* **2007**, *43*, 1219-1225.

(6) Fridovich, I. *Annu. Rev. Biochem.* **1995**, *64*, 97-112.

(7) Kresge, N.; Simoni, R. D.; Hill, R. L. *Jour. Biol. Chem.* **2006**, *281*, e17-e19.

(8) Prabhakar, R.; Vreven, T.; Morokuma, K.; Musaev, D. G. *Biochem.* **2005**, *44*, 11864-11871.

(9) MacFaul, P. A.; Ingold, K. U.; Lusztyk, J. *J. Org. Chem.* **1996**, *61*, 1316-1321.

(10) Valgimigli, L.; Amorati, R.; Fumo, M.; DiLabio, G.; Pedulli, G.; Ingold, K.; Pratt, D. *J. Org. Chem.* **2008**, *73*, 1830-1841.

(11) Snelgrove, D. W.; Lusztyk, J.; Banks, J. T.; Mulder, P.; Ingold, K. U. *J. Am. Chem. Soc.* **2001**, *123*, 469-477.

(12) Litwinienko, G.; Ingold, K. U. *J. Org. Chem.* **2003**, *68*, 3433-3438.

(13) Scaiano, J.; Martin, A.; Yap, G.; Ingold, K. *Org. Lett.* **2000**, *2*, 899-901.

(14) Maillard, B.; Ingold, K. U.; Scaiano, J. C. *J. Am. Chem. Soc.* **1983**, *105*, 5095-5099.

(15) Bejan, E. V.; Font-Sanchis, E.; Scaiano, J. C. *Org. Lett.* **2001**, *3*, 4059-4062.

(16) Ballester, M. *Acc. Chem. Res.* **1985**, *18*, 380-387.

(17) Frenette, M.; Aliaga, C.; Font-Sanchis, E.; Scaiano, J. C. *Org. Lett.* **2004**, *6*, 2579-2582.

(18) Frenette, M.; MacLean, P. D.; Barclay, L. R.; Scaiano, J. C. *J. Am. Chem. Soc.* **2006**, *128*, 16432-16433.

(19) Laidler, K. J.; Meiser, J. H. *Physical Chemistry (3rd ed.)*; Houghton Mifflin Company: Boston, 1999.

(20) Frenette, M. *Advances in Free Radical Oxidation: Mechanistic Studies, Fluorescent Probe Design and Radically Different Antioxidants.*; Doctoral Dissertation, University of Ottawa: Ottawa, Canada, 2008.

(21) Barclay, L. R. C. *Can. J. Chem.* **1993**, *71*, 1-16.

(22) Hatfield, G. L.; Barclay, L. R. *Org. Lett.* **2004**, *6*, 1539-1542.

(23) Howard, J.; Ingold, K. *Can. J. Chem.* **1962**, *40*, 1851-1864.

(24) Abraham, M. H.; Grellier, P. L.; Prior, D. V.; Morris, J. J. *Perkin Trans. 2* **1990**, 521-529.

(25) Abraham, M.; Buist, G.; Grellier, P.; McGill, R.; Prior, D.; Olivier, S.; Turner, E.; Morris, J.; Taylor, P.; Nicolet, P.; Maria, P.-C.; Gal, J.-F.; Abboud, J.-L. M.; Doherty, R.; Kamlet, M.; Shuely, W.; Taft, R. *J. Phys. Org. Chem.* **1989**, *2*, 540-552.

(26) Howard, J. A.; Ingold, K. U. *Can. J. Chem.* **1964**, *42*, 1044-1056.

3 Oxidation of Copper Nanoparticles: Kinetic and Mechanistic Investigations

3.1 Introduction to Nanoparticles

In the past decade there has been an explosion of research interest in the field of nanomaterials. In particular, metal nanoparticles have received much attention due to their diverse potential applications, stemming from the special properties that arise when a bulk metal is reduced in size to nanoscale particles, generally ranging from 1 nm to 100 nm in diameter[1,2].

Many of these special properties are a result of very high surface area-to-volume ratios of nanoparticles, which cause significant surface energy instability. This leads to melting point depletion and higher reactivity than that of the same bulk material[1,3]. For example, the melting point of 1 nm gold and copper nanoparticles is less than 1000 K, compared to much higher bulk gold[4] (1337 K) and copper[5] (1358 K) melting temperatures.

Some noble-metal nanoparticles also exhibit unique optical effects, such as the Surface Plasmon Resonance (SPR) band. The SPR is caused by the coherent oscillation of the conduction band electrons that interact with an electromagnetic field[1]. When the coherent electron motion in the nanoparticle is in resonance with the electromagnetic field, an SPR absorption band is detected. The SPR absorption depends on the size, shape, and surrounding medium of the nanoparticles. For example, spherical gold nanoparticles, ~10 nm in diameter, have a maximum SPR absorption at ~520 nm in water[6].

Applications for metal nanoparticles are very diverse, ranging from electronics and biotechnology to diagnostic imaging and materials science[7-9]. For example, gold nanoparticles are used in biosensors for diagnosing lung cancer from exhaled breath[10,11]. Silver nanoparticles are added to fabrics to make clothing, socks, and hospital sheets with antibacterial properties[12]. Taking advantage of their melting point decrease, nanoparticle inks can be produced to print conductive patterns for electronic devices[13]. The high surface area-to-volume ratio and increased reactivity of nanoparticles also make them the subject of strong interest in the field of catalysis[2,14].

Copper nanoparticles (CuNP) are attracting increasing attention due to their potential applications in electronic and optical devices[13,15,16], where they could be used as a substitute for gold and silver, which would lead to considerable cost reductions. Other important uses for CuNP lie in the field of catalysis[14,17,18].

At the present time, the main limitation for using CuNP is their instability under air due to oxidation. One way to prevent CuNP oxidation is to add stabilizers, such as polyvinylpyrrolidone (PVP)[19]. However, since relatively high stabilizer concentrations are required, the stabilizer may potentially interfere with the chemistry of CuNP through steric hindrance. Therefore, other approaches for preventing CuNP oxidation are desirable.

Detailed understanding of this oxidative process is necessary in developing strategies for CuNP stabilization. We used techniques such as UV-visible

spectroscopy, oxygen uptake measurements and electron paramagnetic resonance (EPR) spectroscopy to gain insight into the mechanism of CuNP oxidation.

This was a collaborative project within our group, and thus some of the experiments discussed were performed by a post-doctoral fellow, Dr. Natalia Pacioni, and by an Honour's project student who I co-supervised, Nathalie Presseau[20].

3.2 Photochemical Synthesis of CuNP

A variety of approaches have been developed for CuNP synthesis. Most of them are chemical reduction methods of copper salts by hydrazine[21] or sodium borohydride[22], in the presence of stabilizers[19], or surfactants that form micelles[22] or that act as capping agents.

Being primarily a photochemistry laboratory group, we have used a photochemical route for the synthesis of CuNP. This method was first developed for the preparation of gold nanoparticles[6] (AuNP), and recently has been successfully adapted for aqueous CuNP synthesis by Dr. Natalia Pacioni[23]. The key feature of this technique is photogeneration of the reducing species through UV light irradiation of a precursor species. A family of compounds called Irgacures proved to be suitable for this task (Scheme 3.1). Upon irradiation with UV light, these compounds undergo Norrish type I cleavage to generate active reducing agents – the Irgacure-2959 (I-2959) yields ketyl radicals, whereas the Irgacure-907 (I-907) produces α-amino alkyl radicals, which have even stronger reducing power. A variety of Irgacures can be obtained from CIBA, and the Irgacure of choice, as well as the type of UV light and the copper salt used, depends on the experimental conditions and the desired effect.

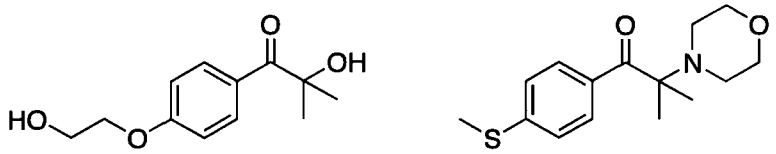

I-2959 I-907

Scheme 3.1 Irgacures used as precursors of reducing species for CuNP synthesis.

For example, I-907 is soluble in organic solvents and is used in the Scaiano group for CuNP synthesis in organic media, particularly acetonitrile. The I-2959 is soluble in water, and is suitable for aqueous CuNP synthesis. Varying the wavelength of irradiation changes the properties of the nanoparticles. For example, UVB irradiation (300 nm lamps), where Irgacures absorb most strongly, leads to very rapid CuNP synthesis, but greater size variability. Irradiating with UVA light (350 nm), where the Irgacures just start absorbing, leads to slower but more controlled CuNP synthesis, creating more monodisperse nanoparticles.

Monodispersity is a desirable feature for nanoparticles. The key to achieving monodispersity is the ability to separate the nucleation and growth steps, such that nucleation occurs quickly at the beginning, and is then followed by the particle growth[24]. Various factors controlling CuNP synthesis have been studied in the Scaiano group. In particular, the effects of counter-ions of the copper (II) precursor salts on the growth rate and dispersity of the nanoparticles have recently been

analyzed[23]. It was indeed found that the counter-ions greatly influence the CuNP formation. For example, synthesis from $CuSO_4$ produces uniform spherical CuNP, while using $CuCl_2$ as a precursor leads to rapid, but more polydisperse CuNP. The results in the presence of chloride ions are particularly interesting because they suggest a catalytic mechanism for CuNP formation by Cl^-, in which nucleation and growth steps are less separated. Overall, numerous factors can be used to control CuNP synthesis. This photochemical method for nanoparticle preparation is advantageous because it uses mild reaction environments (room temperature, atmospheric pressure), and also provides an additional degree of spatial and temporal control of the synthesis through variations in irradiation conditions.

For the experiments discussed in this chapter, aqueous CuNP are used. Copper sulfate ($CuSO_4$) is the nanoparticle precursor because it has been found to yield nanoparticles of highest monodispersity and shape uniformity. The synthesis is performed under argon at room temperature with 30-minute UVA irradiation period (*Experimental Section*).

In the case of these CuNP, we used I-2959 in a reaction displayed in Scheme 3.2. The generated ketyl radical is then able to reduce Cu^{2+} to Cu^+. Eventually, Cu^+ reduces to Cu^0 either through disproportionation reactions or with the help of another ketyl radical. The Cu^0 then undergo nucleation, followed by growth, which leads to the formation of CuNP.

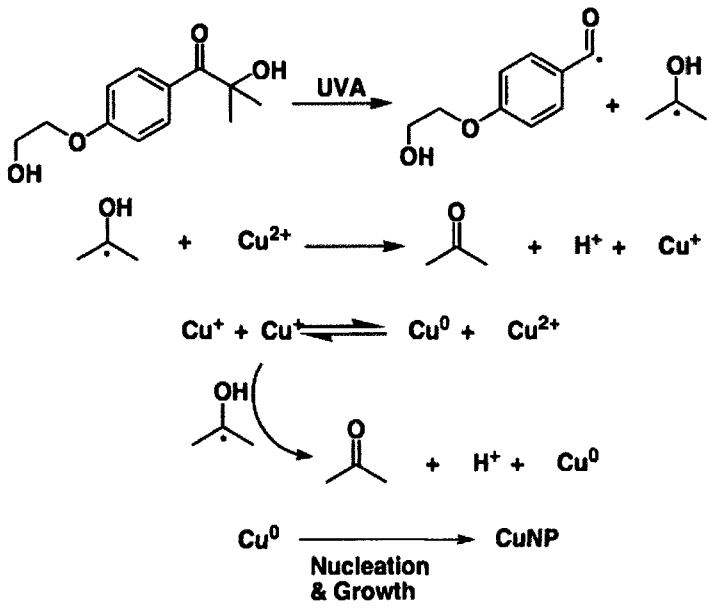

Scheme 3.2 Photochemical route to the synthesis of CuNP.

During this reaction, the sample undergoes a colour change from clear to opaque reddish-brown. The resulting CuNP were mainly characterized by UV-visible spectroscopy, where the characteristic SPR band is detected at 575 nm (Figure 3.1). The absorption below ~360 nm is due to the I-2959. Sometimes, during nanoparticle synthesis, the absorption at higher wavelengths (>700 nm) increases as well. This may be attributed to scattering due to nanoparticle shape and size variation, and also to copper oxide formation on the nanoparticle surface[25]. For these CuNP, however, the residual high-wavelength absorbance is usually quite low. The resulting nanoparticles are generally spherical and quite monodisperse, with an average size of 8.2 ± 0.1 nm, as can be seen by SEM imaging (Figure 3.2).

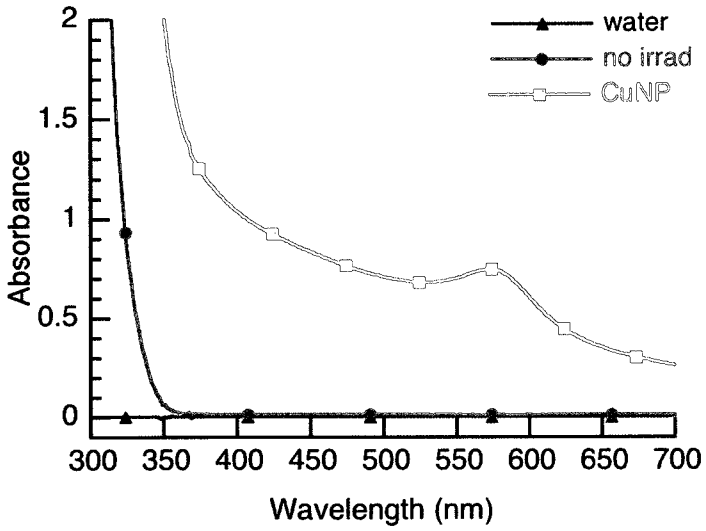

Figure 3.1 **UV-visible absorbance of CuNP synthesized from 0.66 mM $CuSO_4$ and 1.3 mM I-2959 in water at room temperature after 30 minute UVA (350 nm) irradiation.**

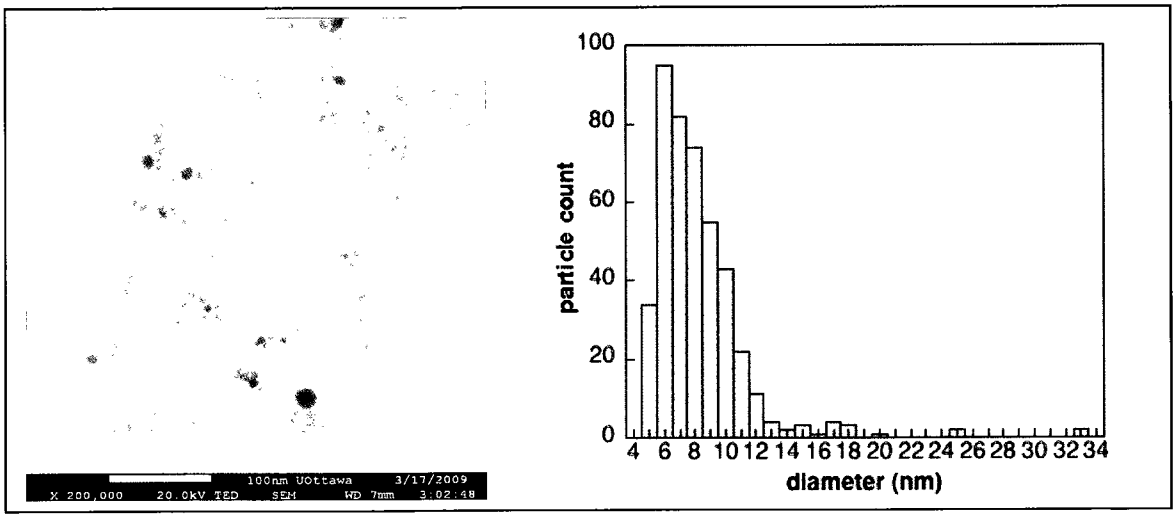

Figure 3.2 (A) SEM image of CuNP synthesized from $CuSO_4$ precursor. Scale bar is 100 nm; (B) Histogram indicating average particle size of 8.2 ± 0.1 nm, calculated for 478 nanoparticles.

3.3 CuNP Instability under Air

As previously mentioned, the major challenge in CuNP applications is their oxidative degradation under air. The goal of the studies discussed in this chapter is to gain insight into the mechanism of CuNP oxidation, which would help in developing new approaches for CuNP stabilization.

In the absence of oxygen, the CuNP are stable for weeks. Upon exposure to air, however, they quickly oxidize, as seen by the disappearance of the SPR peak in the UV-visible absorbance spectra (Figure 3.3). Under these conditions, oxidation takes at least two hours. In this experiment, the CuNP sample in a cuvette containing a small magnetic stirring bar, was opened to air and the absorbance was

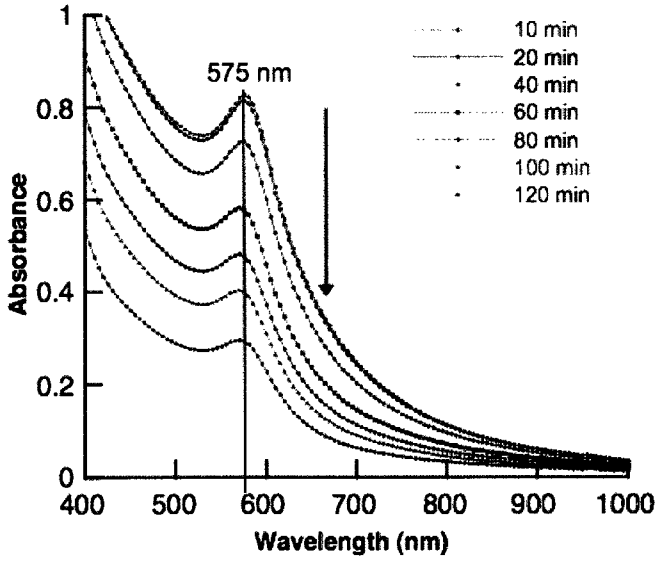

Figure 3.3 UV-visible absorbance spectra of CuNP upon exposure to air.

measured during the indicated intervals. The subsequent question arises about the nature of CuNP oxidation, namely – is oxygen being consumed, or is it being used in some form of electron transfer mechanism?

To test this, we have turned to the oxygen uptake apparatus, and were able to successfully detect oxygen consumption by CuNP. We have determined the oxygen uptake rate to be up to 8.9 μM/min, with a total O_2 consumption of 196 μM. The oxidation was complete in approximately 22 minutes. In this experiment, CuNP were prepared as described above, by irradiating 0.66 mM $CuSO_4$ and 1.3 mM I-2959 with UVA light for 30 minutes. For the oxygen uptake measurements, a 2 mL aliquot of the resulting CuNP solution was injected into an empty sample cell of the oxygen uptake apparatus, and an oxygen uptake curve was obtained (Figure 3.4). The reference cell contained 2 mL of water and was always maintained in the presence of air. A control experiment was always performed to account for the fact that the reference cell was under air, whereas the CuNP solution was opened to air just before injection into the sample cell (Experimental Section, Figure 3.16). For the control, 2 mL of de-aerated water was injected into the sample cell, and the slope of this resulting curve was subtracted from the subsequent runs, done on the same day.

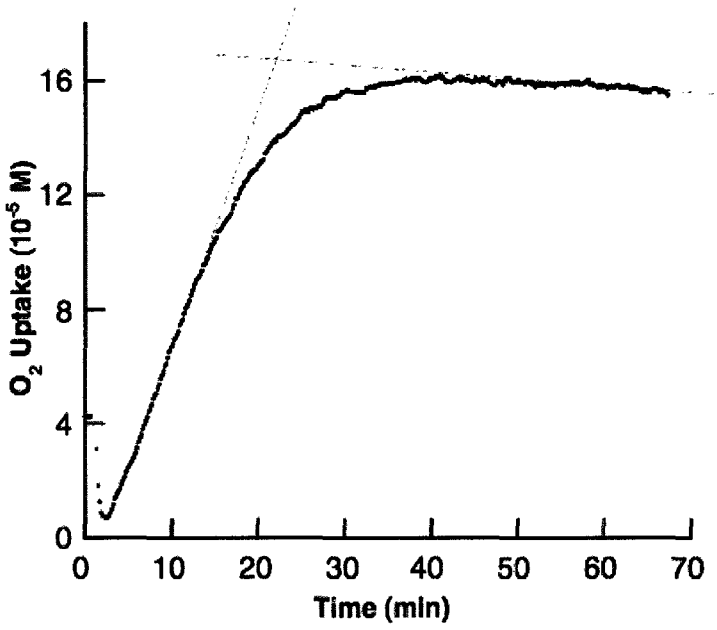

Figure 3.4 An example of an oxygen uptake curve for CuNP oxidation at 30°C.

The results are quite different when the oxidation is followed by monitoring SPR depletion with UV-visible absorbance. In that case, the CuNP oxidation takes a much longer time – approximately 3 hours (Figure 3.5). This discrepancy is attributed to the difference in sample stirring when using these instruments. With the UV-visible spectrometer, a small magnetic stirring bar is used, while the oxygen uptake apparatus is set up to provide constant vigorous stirring of the whole sample, thus constantly replenishing the oxygen supply in the solution. An experiment was performed to illustrate the dependence of stirring on oxidation time, where the sample cuvette was manually shaken between traces, leading to faster CuNP oxidation (Figure 3.6).

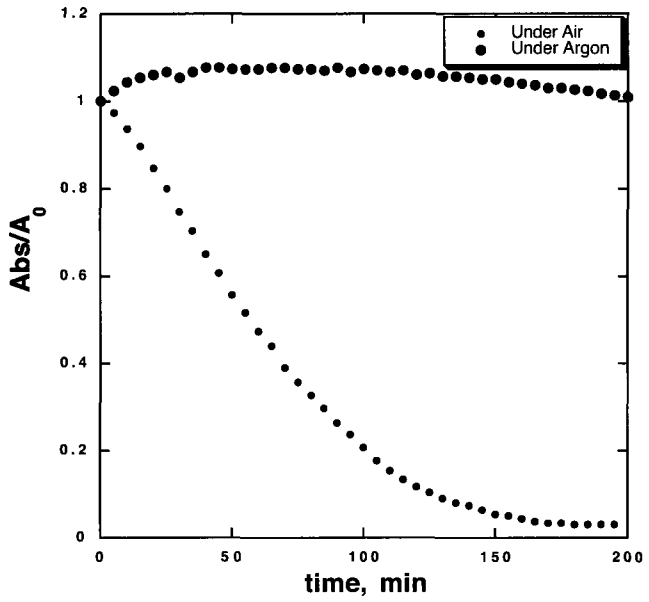

Figure 3.5 UV-visible absorbance of CuNP oxidation over time, monitored at 575 nm, in the absence and presence of air at 30°C.

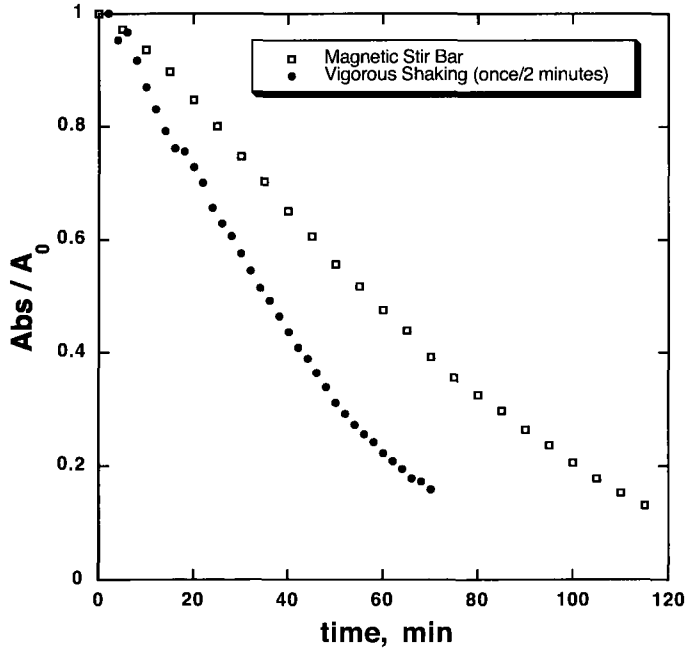

Figure 3.6 Increase of oxidation rate of CuNP with more vigorous stirring. Absorbance monitored at 575 nm.

3.4 Where do the CuNP go?

Visually, during CuNP oxidation, the sample undergoes a colour change from reddish-brown to clear, translucent. In the event of metal oxide formation, one would expect to see a red precipitate for cuprous oxide (Cu_2O) or a black precipitate for cupric oxide (CuO). Another oxidation product, CuOH, is known to absorb at ~470 nm[26]. This peak is not detectable in our experiments because the scattering from the CuNP SPR absorbance obstructs this region of the spectrum (Figure 3.7A). However, the CuOH formation is not expected at the low pH that results from the I-2959 reaction in our experiments[26,27]. Since no precipitate is observed, metal oxides are likely not formed, and the oxidation product is probably the reversion to Cu^{2+}.

To clarify this hypothesis, studies using Electron Paramagnetic Resonance spectroscopy (EPR) were performed. Copper has two common oxidation states – a less stable copper (I), Cu^{+}, and a more stable copper (II), Cu^{2+}. The electronic configuration of Cu^{+} is a filled, d^{10}, shell with no unpaired electrons, and is thus undetectable by EPR. The Cu^{2+}, on the other hand, has a d^{9} electron configuration, and therefore shows an EPR signal.

The experiment was to see if, under our experimental conditions, we could track the Cu^{2+} throughout the CuNP formation and oxidation process. The results of one such experiment are displayed in Figure 3.7. Prior to irradiation of the

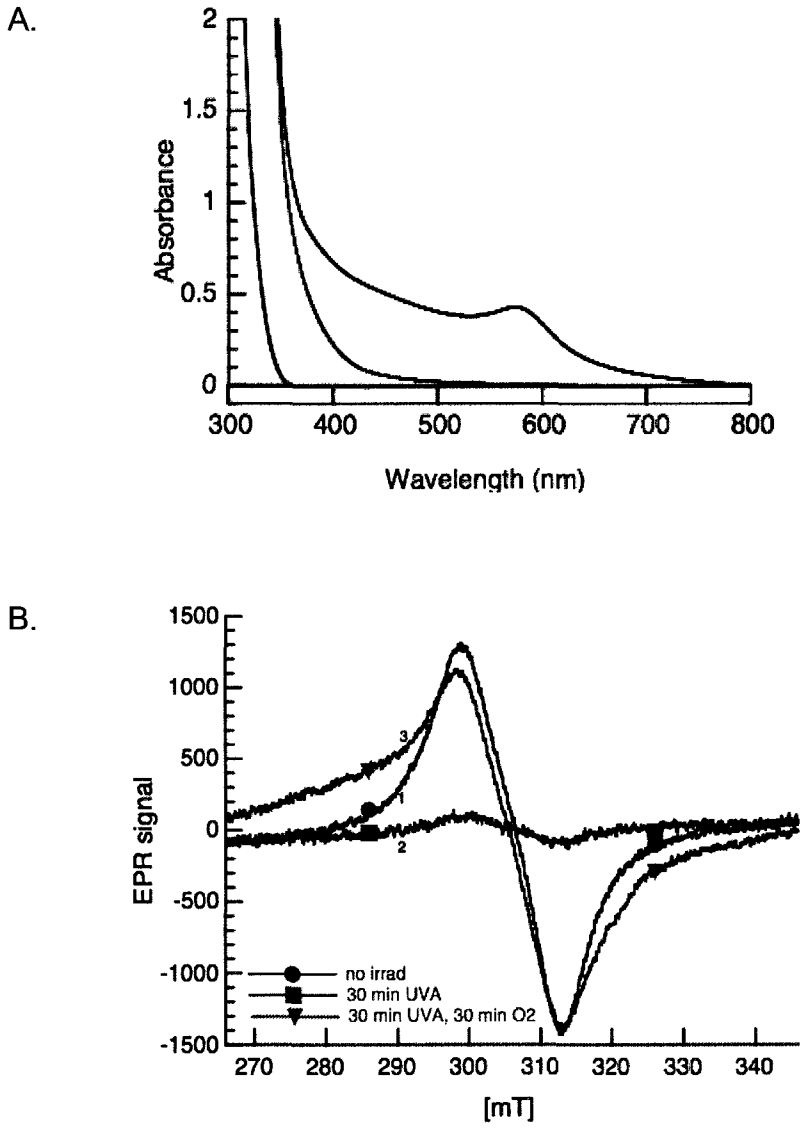

Figure 3.7 UV-visible absorbance (A), and EPR (B) spectra of 0.66 mM $CuSO_4$ + 1.3 mM I-2959 reaction mixture; non-irradiated (blue), after 30 min UVA (red), after 30 min UVA followed by 30 min O_2 purging (green). All spectra recorded at room temperature under argon.

nanoparticle reaction mixture, the $CuSO_4$ signal can be readily detected (blue). With UVA irradiation, the EPR signal diminishes as the copper is reduced to form CuNP (red). Although the signal is greatly reduced, it does not entirely disappear,

indicating incomplete conversion to Cu^0, i.e. the presence of some residual Cu^{2+} after the CuNP formation is finished. The CuNP were then oxidized by purging with oxygen gas for 30 minutes, during which time the solution changed colour from reddish-brown to clear, indicating degradation of the nanoparticles. The sample was then re-purged with argon for 30 minutes before obtaining the UV-visible absorbance and EPR traces (green). The UV-visible absorbance shows absence of CuNP, and the shift to high absorbance below ~400 nm is due to the I-2959 photodegradation products. The EPR shows regeneration of the Cu^{2+} signal, indicating that the CuNP oxidation product is indeed Cu^{2+}.

We estimated the residual Cu^{2+} concentration by integrating the Cu^{2+} signal of the precursor solution and the remaining signal once the CuNP have been formed. In particular, we integrated the EPR signal of the non-irradiated sample, for which the Cu^{2+} concentration is known to be 0.66 mM (integrated signal intensity = 202.86, blue trace in Figure 3.7). We then integrated the signal in the CuNP sample (integrated signal intensity = 1.53, red trace in Figure 3.7), and calculated the residual Cu^{2+} concentration by cross-multiplication. Thus, assuming a direct relationship between the signal intensity and concentration, the estimated residual Cu^{2+} was found to be 0.005 mM. However, this result was not reproducible, and there are several explanations for this. Partially, it may be due to the variable nature of nanoparticle formation, where every nanoparticle batch is slightly different. The other cause for the variability appears to be experimental. We are using a highly dielectric solvent (water): dielectric solvents can absorb microwaves, causing the

sample to overheat if a regular EPR tube is used. We must use a special "flat cell" when running EPR experiments in dielectric solvents. This cell is very thin (0.3 mm), thus reducing the pathlength of microwaves through the sample, thereby preventing sample overheating. The difficulty with this special cell is that its position is not fixed inside the EPR cavity, and once the cell is removed (as it must be when changing samples), it is hard to replace the cell into exactly the same position. Small changes in cell positioning can sometimes lead to quite large changes in the EPR signal. Ideally, another cell that fits precisely into a fixed position in the EPR cavity should be obtained. Then, it will be possible to confirm the acquired results. It would also be interesting to run a standard curve with various Cu^{2+} concentrations and ensure the expected linear relationship with the Cu^{2+} EPR signal.

To obtain the g-value for the Cu^{2+} signal in our reaction mixture, we used a manganese (Mn) standard for EPR. The standard is a white Mn powder in a sealed glass tube that is inserted into the instrument along with the sample, so that a spectrum with both signals is obtained. In EPR, Mn shows six sharp, distinct peaks. Since each peak has a known position (g-value), any one of the six can be used as a reference for determining the g-value of the signal in one's sample. The g-value for the Cu^{2+} signal in our experiments was found to be 2.212, which is quite high. This g-value is comparable to those reported for other copper (II) compounds in solution at room temperature[28].

3.5 Ascorbic Acid for CuNP stabilization

To try and prevent the CuNP oxidation reaction, we decided to employ molecules that are known to do so – antioxidants. Since we are working in an aqueous system, such was the antioxidant of choice, as well. One of the first common water-soluble small-molecule antioxidants that comes to mind is L-ascorbic acid (Vitamin C). L-ascorbic acid is an important antioxidant *in vivo*, where it plays a role in various biological processes, such as Vitamin E recycling[29]. L-ascorbic acid oxidation has been studied for many decades[30,31], and is known to proceed *via* a two-step process, donating electrons until finally resulting in dehydroascorbate[32] (Scheme 3.3). In addition, it is well known to reduce transition metal complexes[30].

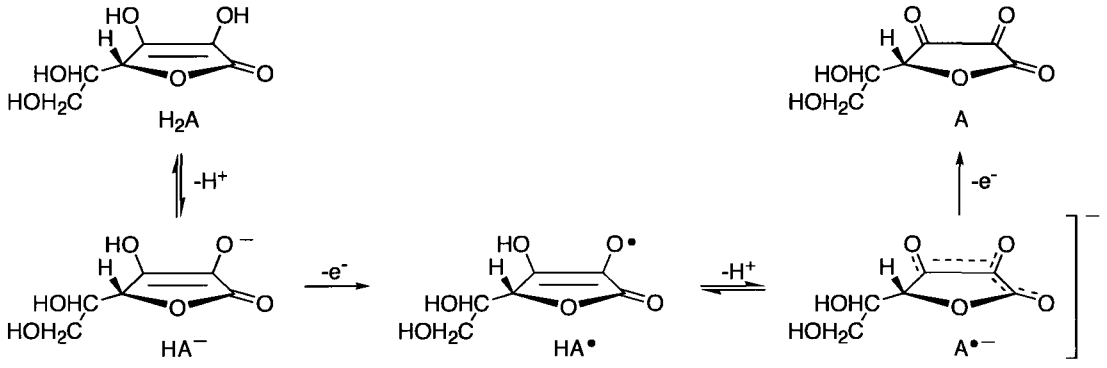

Scheme 3.3 Oxidation of L-ascorbic acid.

This excellent reducing ability has also made ascorbic acid useful in nanoparticle preparation methods, particularly for silver and gold, where it is used as the reducing agent[33,34].

Addition of ascorbic acid to CuNP indeed results in slowing down the CuNP oxidation – the oxidation is not stopped, but rather an induction period is established. The UV-visible absorbance results show that the CuNP are oxidized in 3 hours without ascorbic acid, whereas addition of 1 mM ascorbic acid extends CuNP existence to over 6 hours. In this experiment, the SPR band was monitored by UV-visible absorbance in the absence and in the presence of 1 mM ascorbic acid (Figure 3.8). It was also found that CuNP oxidation is slowed down at lower temperatures (results not shown).

We also studied the effect of ascorbic acid on CuNP with EPR spectroscopy (Figure 3.9). In this experiment, 1 mM ascorbic acid was added to CuNP in the absence of oxygen, and the residual Cu^{2+} signal that is present in the CuNP solution was monitored over time by EPR. The first measurement was taken 6 minutes after ascorbic acid addition because this was the time it took to transfer the sample into the EPR cell, and move it from the glovebox into the EPR instrument. Subsequently, measurements were taken every 15 or 30 minutes, up to 90 min (that is, 96 minutes after ascorbic acid addition). Throughout this time, a decrease in the residual Cu^{2+} signal, and therefore in Cu^{2+} concentration, was observed. These results suggest that, in a de-aerated solution, ascorbic acid reacts with Cu^{2+}, and

most likely reduces it to Cu^+ (*vide infra*). An increase in Cu^+ concentration could lead to a higher probability of Cu^+ disproportionation to Cu^0. This means that, in the presence of oxygen, ascorbic acid could be stabilizing CuNP by favouring formation of more Cu^0 that could attach to existing CuNP, thus slowing down CuNP oxidation. It is important to note that the EPR cell was not moved during this period, thereby eliminating the possibility of changing signal while re-positioning the cell.

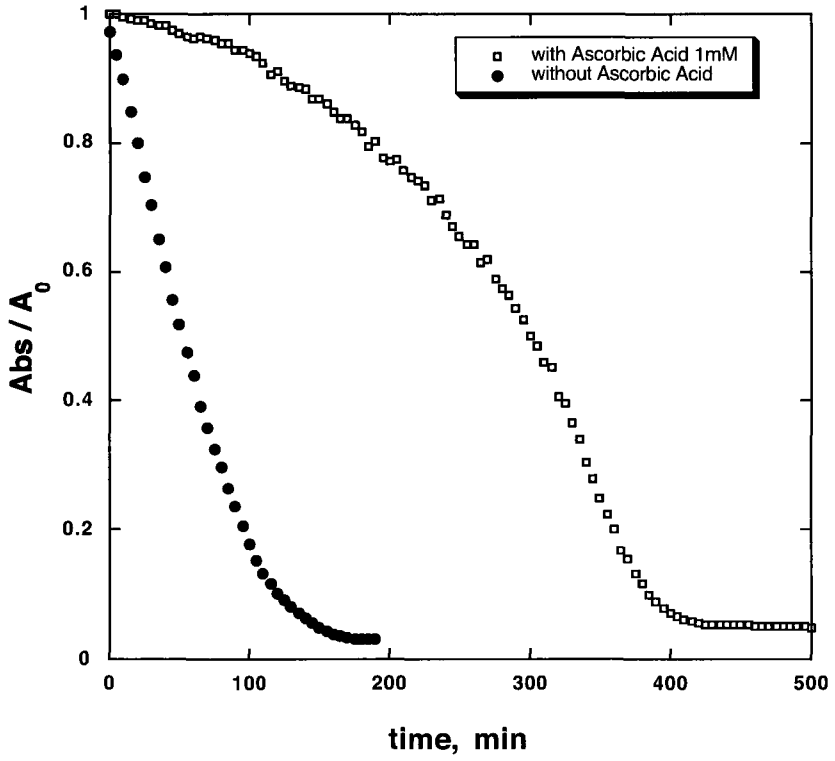

Figure 3.8 Effect of 1 mM ascorbic acid on oxidation of CuNP under air at 30°C. Monitoring absorbance at λ = 575 nm.

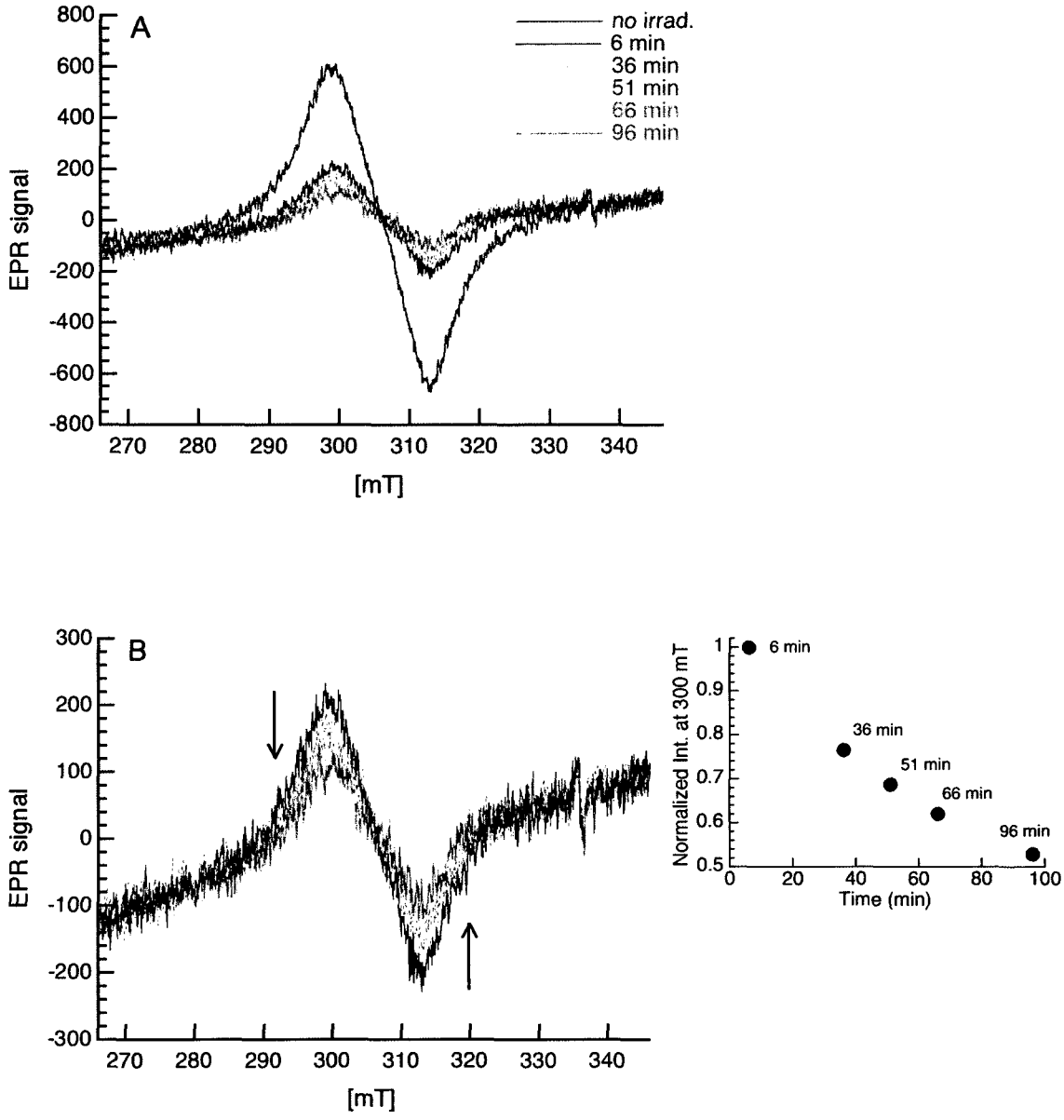

Figure 3.9 (A) EPR of CuNP monitored over time after addition of 1 mM ascorbic acid in absence of oxygen at room temperature. CuNP were prepared by 30 min *UVA irradiation of aqueous solution of 0.66 mM $CuSO_4$ and 1.3 mM* I-2959; (B) Expansion of residual Cu^{2+} signal region. Arrows indicate trend observed. Inset: Normalized EPR signal intensity at 300 mT vs. time after ascorbic acid addition.

We also wanted to see if the oxygen uptake of CuNP would decrease in the presence of ascorbic acid, as well. Surprisingly, the oxygen consumption was instead found to dramatically increase after the addition of ascorbic acid (Figure 3.10). The rate of oxygen uptake of CuNP together with 1 mM ascorbic acid was found to be ~122 μM O_2/min, which is a greater than 15 fold increase from the oxidation rate of just CuNP. The oxidation was complete in ~8 minutes, resulting in a total consumption of ~975 μM O_2. The oxygen uptake results together with the UV-visible results in Figure 3.8 are an indication that ascorbic acid is a sacrificial

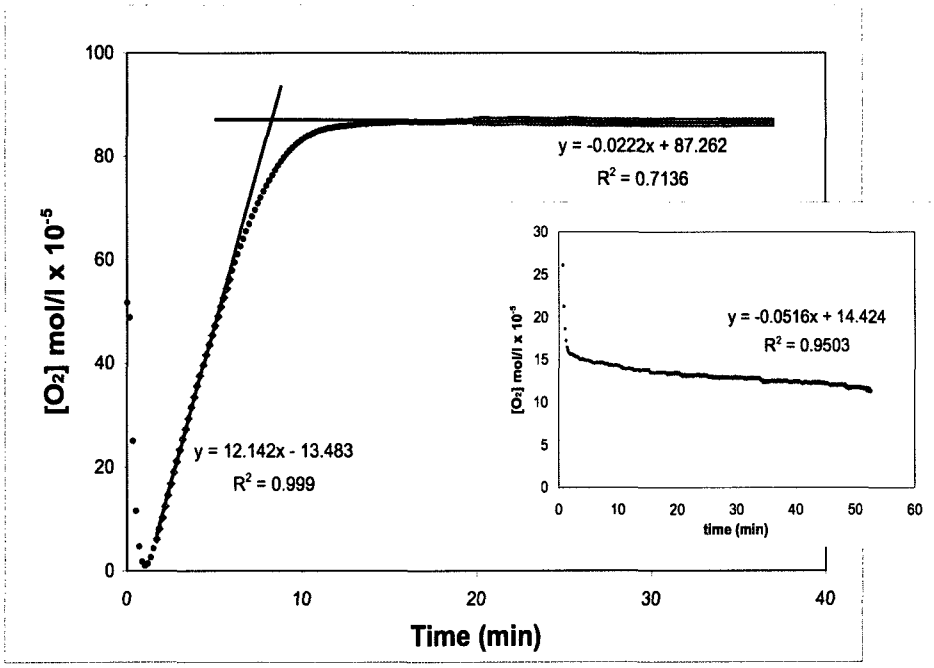

Figure 3.10 Oxygen uptake of CuNP sample in the presence of 1 mM ascorbic acid at 30°C.

stabilizer of CuNP, and that the addition of CuNP initiates a catalytic cycle that consumes molecular oxygen.

These oxygen uptake results also suggest a catalytic mechanism for ascorbic acid oxidation. The question now became – could the CuNP be the catalyzing species, making this ascorbic acid oxidation reaction an example of nanoparticle catalysis?

3.6 Catalysis of ascorbic acid oxidation

It has been well established that copper (II), along with iron (III), is a catalyst of ascorbic acid oxidation[35-37]. Do CuNP also have this capability, and if so, how efficient are they? To our knowledge, the role of nanoparticles in this reaction has not been previously investigated.

Several oxygen uptake experiments, exploring the properties of ascorbic acid oxidation with CuNP and Cu^{2+} were performed. The results from oxygen uptake experiments comparing only CuNP, CuNP with 1 mM ascorbic acid, and precursor reaction mixture without irradiation (i.e. containing 0.66 mM $CuSO_4$ and 1.3 mM I-2959) are displayed in Figure 3.11. From these curves it is evident that Cu^{2+} is faster at catalyzing ascorbic acid oxidation compared to the CuNP solution. However, it is important to keep in mind that the concentration of CuNP produced from this precursor solution is much less than 0.66 mM. Notice that the total amount of oxygen uptaken in the case of CuNP + 1 mM ascorbic acid (blue trace) is higher than that of Cu^{2+} + 1 mM ascorbic acid (black trace) roughly by the amount due to CuNP oxidation (green trace).

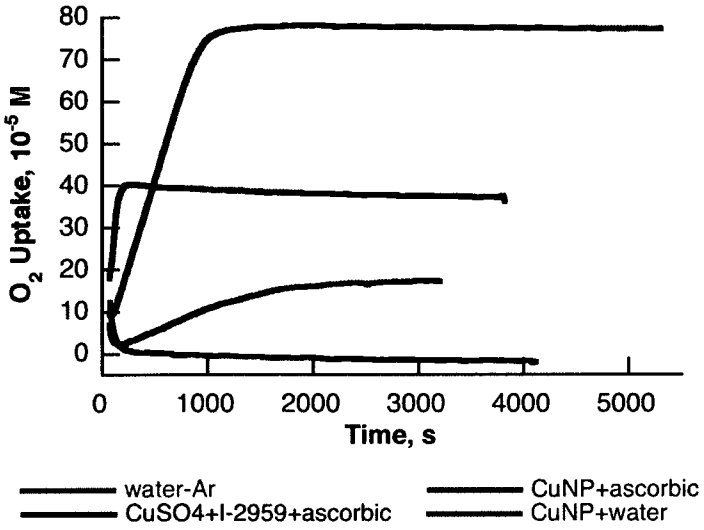

Figure 3.11 Oxygen uptake of CuNP in the absence and presence of 1 mM ascorbic acid, and of non-irradiated precursor reaction mixture in the presence of 1 mM ascorbic acid. Reaction temperature is 30°C.

Other studies of this reaction were conducted, in which ascorbic acid concentration was varied in the presence of CuNP (Figure 3.12). In another study, the ascorbic acid concentration was kept constant, while the copper sulfate concentrations differed (Figure 3.13). These results show that the amount of oxygen uptaken is dependent on the amount of ascorbic acid present, and the rate of oxygen uptake depends on the amount of copper (II) present.

The question still remained of whether CuNP are able to catalyze ascorbic acid oxidation, as a proof of concept of photochemically synthesized, unprotected nanoparticle catalysis. Or, alternatively, is there enough of the residual Cu^{2+} present in the CuNP to account for the catalytic oxidation observed? From the EPR

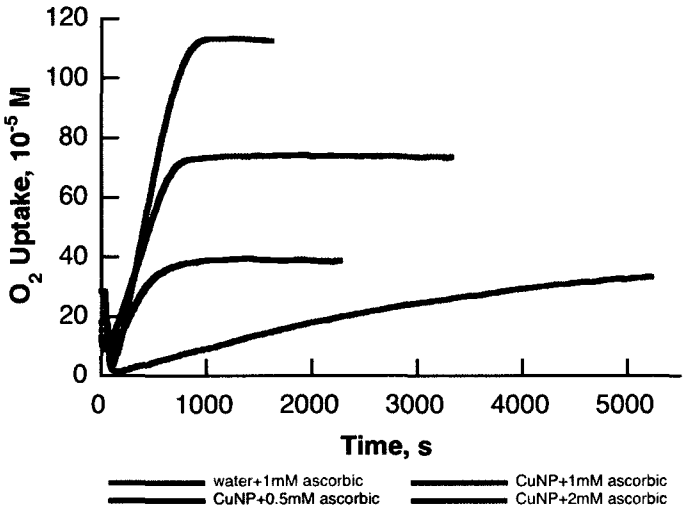

[Asc] (mM)	O_2 uptake rate (μM/s)	Oxid. time (min)	O_2 consumed
1 (control)	0.10	~45 (slows)	N/A
0.5	0.78	9	0.41 mM
1	1.09	11	0.74 mM
2	1.75	13	1.16 mM

Figure 3.12 CuNP with varying ascorbic acid concentrations in water at 30°C.

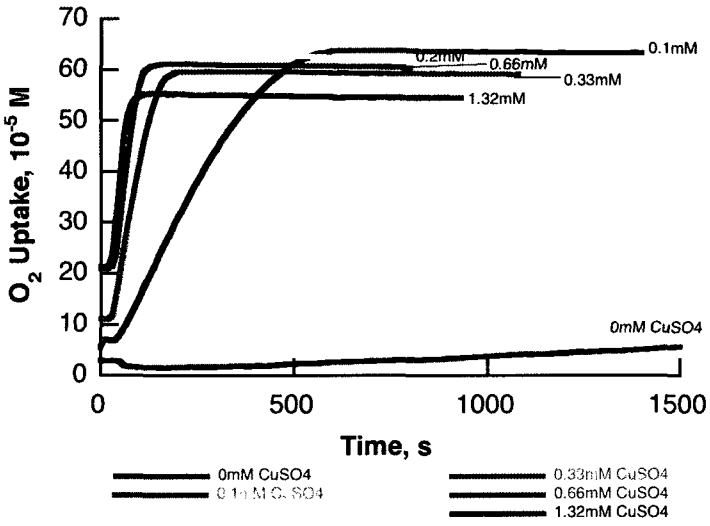

[CuSO4] (mM)	O_2 uptake rate (μM/s)	Oxid. time (min)	O_2 consumed
0	0.04	N/A	N/A
0.10	1.29	6.0	0.64 mM
0.20	3.33	3.2	0.63 mM
0.33	4.14	2.4	0.60 mM
0.66	6.03	1.7	0.61 mM
1.32	7.81	1.2	0.55 mM

Figure 3.13 Varying copper sulfate concentrations with 1.3 mM I-2959 and 1 mM ascorbic acid in water at 30°C.

results previously discussed (section 3.4, Figure 3.7), it is tempting to conclude that CuNP are responsible in part for the catalysis, because a Cu^{2+} concentration of 0.005 mM is too low to entirely account for the observed catalytic reaction. However, the major challenge is to reliably measure the residual Cu^{2+} concentration.

Since the amount of residual Cu^{2+} is quite variable in each CuNP synthesis, we performed an EPR experiment together with oxygen uptake. The idea was to first quantify the residual Cu^{2+} of a CuNP batch, and then use these particular nanoparticles in an oxygen uptake experiment with 1 mM ascorbic acid. Then, redo the experiment, again with 1 mM ascorbic acid, but now prepare a Cu^{2+} sample containing the same Cu^{2+} concentration as the "residual concentration" predicted by EPR. The goal is to clarify if, when using CuNP, the catalysis observed is due to the nanoparticles, or merely to the residual Cu^{2+} present. From Figure 3.14 we see that the simulated residual Cu^{2+}, which in this experiment was found to be 0.076 mM, is enough to catalyze ascorbic acid oxidation, and the catalysis is actually faster than when CuNP are used. However, in this experiment, the EPR cell had to be moved between acquisitions, and although care was taken to replace it into the same position, the signal could have been altered, and perhaps the 0.076 mM residual Cu^{2+} concentration measured is higher than the actual value. Therefore, more experiments are needed to determine the final answer to this question. In particular, we must ensure a reliable determination of the residual Cu^{2+} concentration. Nevertheless, these results suggest that when CuNP are used, the ascorbic acid oxidation observed is likely due to the presence of residual Cu^{2+}.

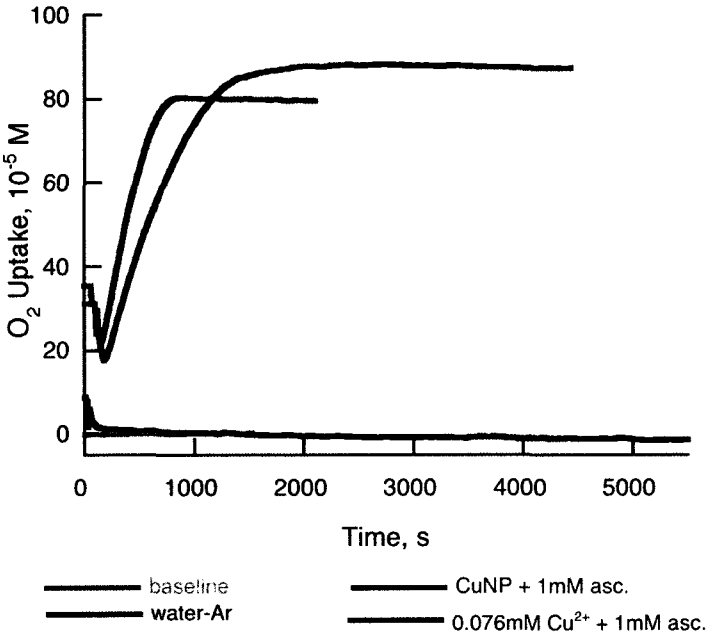

Figure 3.14 Oxygen uptake of samples containing 1 mM ascorbic acid and either CuNP, or a simulated concentration of residual Cu^{2+} (0.076 mM $CuSO_4$), as determined by EPR.

3.7 Is Cu^+ present as an intermediate?

For studying CuNP oxidation, another important step is to determine whether, on the way to Cu^{2+}, the CuNP go through a Cu^+ intermediate. As mentioned earlier, copper (I) is a much less stable species than copper (II). One of the ways to detect copper (I) is by trapping it. For this purpose, we used Neocuproine, a compound that binds specifically to Cu^+ and forms a very stable complex. The resulting complex is bright yellow with a maximum absorption at 450 nm, and is readily detected by UV-visible absorbance spectroscopy (Scheme 3.4).

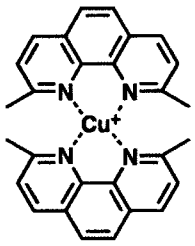

Scheme 3.4 Neocuproine complexes readily with Cu^+ with λ_{max}~ 450 nm

We conducted an experiment, where neocuproine was added to CuNP when they were just opened to air, and monitored over time by UV-visible spectroscopy. During the CuNP oxidation (seen by decrease of the SPR band at 575 nm), the neocuproine complex could easily be detected (growth of absorbance at 450 nm), thereby proving the presence of Cu^+ during the CuNP oxidation reaction (Figure 3.15).

We also found that addition of ascorbic acid to copper sulfate in the absence of oxygen leads to formation of copper (I), which is indicated by the neocuproine complex detected when neocuproine is present in the reaction mixture (data not shown). No neocuproine complex is detected if ascorbic acid is not added.

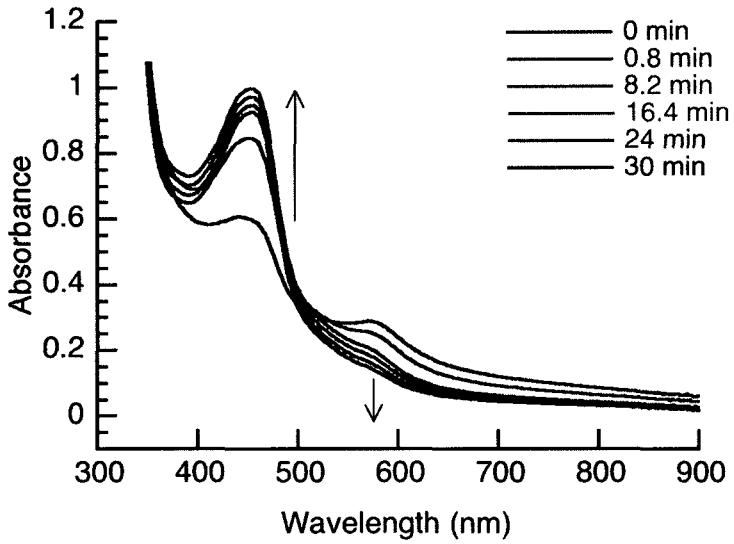

Figure 3.15 UV-visible absorbance of CuNP oxidation in the presence of neocuproine. Note a decrease at 575 nm (CuNP SPR band) and an increase at 450 nm (neocuproine-Cu^{+} complex). Absorbance was monitored at 30 s intervals for 30 min. Select traces are shown for clarity.

3.8 Conclusions

CuNP are unstable in the presence of oxygen, and readily oxidize to form Cu^{2+} as one of the products, with Cu^{+} as one of the intermediates present. Addition of L-ascorbic acid slows down CuNP oxidation, thus extending the lifetime of CuNP. Although ascorbic acid stabilizes CuNP, it itself is oxidized. Thus, ascorbic acid is a sacrificial stabilizer of CuNP. Based on literature[30,36,37] and our results, we propose a mechanism of CuNP stabilization by ascorbic acid, where ascorbic acid plays a role of reducing Cu^{2+} back to Cu^{+}, thereby facilitating the disproportionation reaction to form more Cu^{0}. Essentially, the CuNP oxidation is counteracted by additional formation of Cu^{0}, which may be able to bind to existing CuNP. In this way, the lifetime of CuNP is extended, while ascorbic acid is sacrificed. The Cu^{2+} in this scenario catalyzes the oxidation of ascorbic acid, which is consistent with our results.

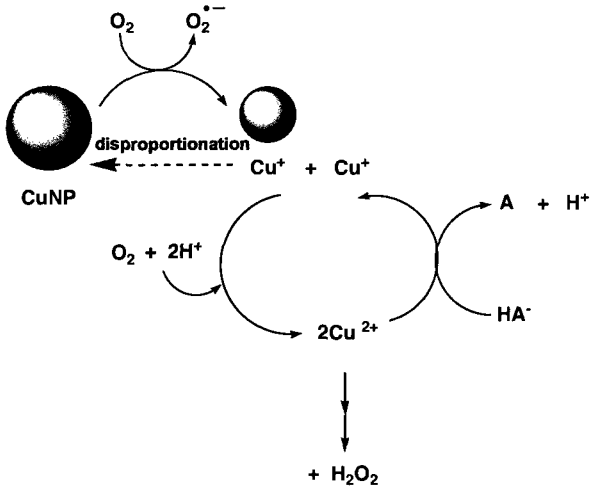

3.9 Experimental Details

3.9.1 Materials

All materials were purchased from Sigma-Aldrich, except where indicated otherwise. Copper (II) sulfate ($CuSO_4$) and L-ascorbic acid were used as received. Irgacure-2959 (I-2959) was a gift from CIBA and was purified by recrystallization in ethyl acetate. All water used was millipore with room temperature resistivity of 18.2 MΩ, obtained from a Milli-Q ultrapure water purification system from Millipore.

For stock solution preparation, ~10 mM $CuSO_4$ and ~10 mM ascorbic acid solutions were prepared without difficulty due to easy solubilization in water. The I-2959 stock (~10 mM) was prepared in a volumetric flask and heated for ~1 hour in a waterbath at ~50-60°C (while stirring with a magnetic stirbar) to aid dissolution, but avoid thermal degradation. Also, the I-2959 solution was stored wrapped in aluminum foil to avoid photodegradation. All stock solutions were stored at room temperature. The ascorbic acid solution was prepared fresh each time and kept wrapped in aluminum foil.

Rubber septa and PTFE tubing (20 gauge) was obtained from Sigma-Aldrich, syringes (Hamilton), quartz cuvettes with a neck (1 cm pathlength), fused quartz EPR flat cell (0.3 mm pathlength), EPR manganese reference (Mn^{2+}/MnO, Jeol Co.), UVA lamps (350 nm, Luzchem), photoreactor (Luzchem).

3.9.2 Copper Nanoparticle Synthesis

The reaction mixture was prepared from stock solutions for a final composition of 0.66 mM $CuSO_4$ and 1.3 mM I-2959 in water. Aliquots of the reaction mixture (3 mL) were placed into quartz cuvettes on which a rubber septum can be fitted, and purged with argon for 30 minutes. To avoid reactions of the purging metal needle with the sample, PTFE tubing was attached to the needle, such that only the tubing came in contact with the reaction mixture. Samples were placed into a marry-go-round carousel to ensure uniform exposure, and irradiated in a photoreactor with 12-14 UVA lamps for 30 minutes (beforehand, the photoreactor lamps were warmed up for 30 minutes).

For experiments with ascorbic acid, the CuNP were prepared with less water, so that the volume would be 3 mL after addition of the required amount of ascorbic acid stock solution. For example, for 1 mM ascorbic acid experiments, usual amounts of $CuSO_4$ and I-2959 were used, but water was added for a final sample volume of 2.7 mL (instead of 3 mL). Thus, the CuNP were synthesized with slightly higher concentrations; >0.66 mM $CuSO_4$ and >1.3 mM I-2959. The concentrations are corrected after 0.3 mL ascorbic acid stock solution (10 mM) is added, for a final concentration of 1 mM ascorbic acid in 3 mL CuNP.

3.9.3 Copper Nanoparticle Characterization

The synthesis of CuNP was verified using UV-visible Spectroscopy. A water baseline (under air) was first obtained. The spectrum of the de-aerated reaction

mixture prior to, as well as after irradiation was obtained, in the same quartz cuvette used for irradiation. The spectra from 300 – 900 nm were usually acquired. CuNP formation is indicated by an SPR peak around 575 nm.

CuNP were also characterized by SEM[23] (Field Emission Scanning Electron Microscope: Jeol, JSM-7500F). Approximately 50 μL of CuNP sample was dropped on a carbon-coated copper grid (400 mesh), and placed under vacuum overnight to evaporate the solvent and remove organic matter.

3.9.4 Monitoring CuNP oxidation by UV-visible absorbance

The samples were exposed to air upon removal of the septum from the cuvette, and a small magnetic stirring bar was added to help oxygen diffusion in the solution. The UV-visible absorbance spectra were obtained in the 400 – 900 nm range. The CuNP oxidation was followed by monitoring the decrease in absorbance of the SPR band, near 575 nm. The experiments were performed in the absence, as well as in the presence, of 1 mM ascorbic acid[20].

3.9.5 Monitoring oxidation with Oxygen Uptake Apparatus

A typical experiment was done as described below. Cells containing 2 mL water were loaded onto the apparatus and equilibrated overnight at 30°C. After performing the pressure check and running the baseline, a control experiment was done with argon-purged water, to account for the pressure change sensed by the apparatus due to argon gas. Water was purged in a cuvette in the same way as the

sample during CuNP synthesis, and equilibrated to 30°C in a waterbath for 5 minutes prior to injection. The sample cell was emptied, dried, and 2 mL of the argon-purged water injected into the sample cell using a syringe and PTFE needle. To mark the time of injection, the chart recorder needle was moved by changing the "R-balance" on the transducer indicator. The cell was re-loaded, and the curve was measured after ~1 minute. The resulting curve (Figure 3.16) typically shows a sharp change in the beginning, where the system is not yet equilibrated (this lasts ~4 minutes). As the environment in the cell stabilizes, the curve becomes flat, with a slight drift due to argon gas, which is present in the sample cell, but not the reference cell. The slope of this control curve was subtracted from the subsequent sample runs, done on the same day.

For the CuNP measurements, the cuvette with the nanoparticles was equilibrated to 30°C in a waterbath for 5 minutes prior to injection. The sample cell was again removed, emptied, dried, and 2 mL of CuNP were injected into the sample cell. The oxygen uptake curve was obtained in the same way as described for the control experiment.

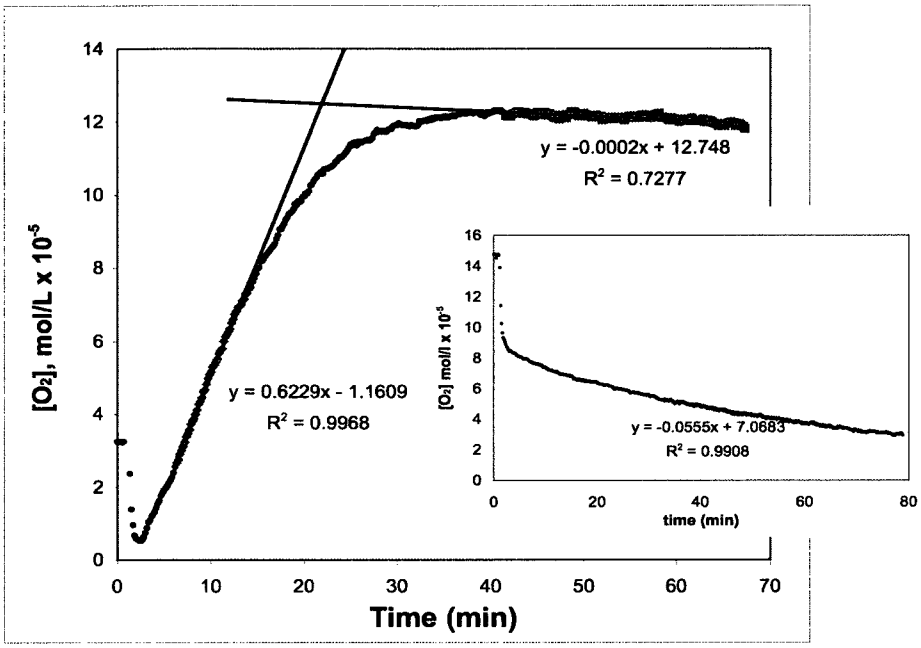

Figure 3.16 Oxygen uptake analysis of CuNP. Pink and blue designate the linear regions used to determine the time of oxidation completion (crossing point of the trendlines). Inset: de-aerated water control; the pink indicates linear region chosen to calculate drift due to argon in the sample cell.

For CuNP experiments with ascorbic acid, a stock solution of ascorbic acid was purged with argon for ~30 minutes, and equilibrated to 30°C as described above. Ascorbic acid was injected into the CuNP (usually to a final ascorbic acid concentration of 1 mM, section 3.9.2) right before starting the oxygen uptake experiments.

3.9.6 EPR spectroscopy of Copper (II)

The EPR measurements were performed with a JEOL FA-100 X-Band EPR spectrometer (Jeol USA, Peabody, MA). The samples were run in a 0.3 mm fused quartz flat cell (Jeol Co.), at room temperature, and in the absence of oxygen. Typical experiments were done as follows. Nanoparticle precursor solution (0.66 mM $CuSO_4$, 1.3 mM I-2959 in water, final volume 6 mL) was prepared in a glass vial, then split into two quartz cuvettes (3 mL in each), and purged with argon for 30 minutes as previously described. One cuvette was irradiated to prepare CuNP, while the other was used to run the EPR spectrum of the precursor solution. EPR spectra were also obtained for the CuNP sample and for the same CuNP sample after it was purged with O_2 for 30 minutes followed by re-purging with Ar for 30 minutes.

To maintain the sample under inert atmosphere, the sample was transferred to the EPR quartz flat cell in a glovebox (LC Technology Solutions Inc.), and sealed with a rubber septum. The EPR spectra were obtained at a frequency of ~9413 MHz. The acquisition parameters were the same for all analyzed samples: Power = 5 mW, Mod. Frequency = 100 kHz, Mod. Width = 1.0 mT, Time constant = 0.03 sec, and Sweep Time = 4 min. Usually, 3 accumulations were obtained.

When using the Mn standard, the Mn peak intensity was chosen to be 500 units.

For the experiment with CuNP and ascorbic acid (

Figure 3.9), non-irradiated and CuNP runs were obtained as described above. For ascorbic acid addition (performed in the glovebox), 50 μL of 20 mM ascorbic acid was added to 1 mL CuNP. The sample was transferred to the EPR flat cell, removed from the glovebox, and EPR measurement taken as quickly as possible. Runs were acquired at 6, 36, 51, 66 and 96 minutes after ascorbic acid addition. EPR acquisition conditions were the same as above, except single accumulations were obtained at each time.

3.9.7 Copper (I) detection with Neocuproine

A neocuproine stock solution, 1.62 mg/mL (ca. 0.26 mM), was prepared in ethanol. Milli-Q water (1.4 mL) and the 0.26 mM neocuproine stock (100 μL) were added to a 1x1 cm quartz cuvette.

To this, 1.5 mL CuNP solution was added and the absorbance spectra was recorded at 30 s intervals for 30 min from 300-900 nm range. An increase of absorbance at 450 was observed over time.

3.10 References

(1) Burda, C.; Chen, X.; Narayanan, R.; El-Sayed, M. *Chem. Rev.* **2005**, *105*, 1025-1102.

(2) Daniel, M.-C.; Astruc, D. *Chem. Rev.* **2004**, *104*, 293-346.

(3) Yeshchenko, O. A.; Dmitruk, I. M.; Alexeenko, A. A.; Dmytruk, A. M. *Phys. Rev. B* **2007**, *75*, 085434.

(4) Hosokawa, M.; Nogi, K.; Naito, M.; Yokoyama, T. *Nanoparticle Technology Handbook*; Elsevier: Oxford, 2007.

(5) Delogu, F. *Phys. Rev. B* **2005**, *72*, 205418.

(6) Marin, M.; McGilvray, K.; Scaiano, J. *J. Am. Chem. Soc.* **2008**, *130*, 16572-16584.

(7) Talapin, D. V.; Lee, J.-S.; Kovalenko, M. V.; Shevchenko, E. V. *Chem. Rev.* **2009**, *(ASAP)*.

(8) Stewart, M. E.; Anderton, C. R.; Thompson, L. B.; Maria, J.; Gray, S. K.; Rogers, J. A.; Nuzzo, R. G. *Chem. Rev.* **2008**, *108*, 494-521.

(9) Homola, J. *Chem. Rev.* **2008**, *108*, 462-493.

(10) Mazzone, P. *Nature Nanotech.* **2009**, *4*, 621-622.

(11) Peng, G.; Tisch, U.; Adams, O.; Hakim, M.; Shehada, N.; Broza, Y. Y.; Billan, S.; Abdah-Bortnyak, R.; Kuten, A.; Haick, H. *Nature Nanotech.* **2009**, *4*, 669-673.

(12) Tarimala, S.; Kothari, N.; Abidi, N.; Hequet, E.; Fralick, J.; Dai, L. L. *J. App. Polym. Sci.* **2006**, *101*, 2938-2943.

(13) Lee, Y.; Choi, J.; Lee, K.; Stott, N.; Kim, D. *Nanotech.* **2008**, *19*, 1-7.

(14) Singh, P.; Katyal, A.; Kalra, R.; Chandra, R. *Catal. Commun.* **2008**, *9*, 1618-1623.

(15) Kruis, F.; Fissan, H.; Peled, A. *J. Aerosol Sci.* **1998**.

(16) Liu, X.; Cai, W.; Bi, H. *J. Mater. Res.* **2002**, *17*, 1125-1128.

(17) Bhadra, S.; Saha, A.; Ranu, B. C. *Green Chem.* **2008**, *10*, 1224-1230.

(18) Nasibulin, A.; Ahonen, P.; Richard, O.; Kauppinen, E.; Altman, I. *J. Nanopart. Res.* **2001**, *3*, 385-400.

(19) Wu, C.; Mosher, B. P.; Zeng, T. *J. Nanopart. Res.* **2006**, *8*, 965-969.

(20) Presseau, N. *Observation of Cu Nanoparticle Oxidation by Spectrophotometry and with Inhibited Oxygen Uptake Method.*; University of Ottawa: Ottawa, 2009.

(21) Wu, S.; Chen, D. *J. Colloid Inteface Sci.* **2004**, *273*, 165-169.

(22) Lisiecki, I.; Billoudet, F.; Pileni, M. *J. Phys. Chem.* **1996**, *100*, 4160-4166.

(23) Pacioni, N. L.; Pardoe, A.; McGilvray, K. L.; Chretien, M. N.; Scaiano, J. C. *Photochem. Photobiol. Sci.* **2010**, *(submitted)*.

(24) Garnweitner, G.; Niederberger, M. *J. Mat. Chem.* **2008**, *18*, 1171-1182.

(25) Pileni, M. *New J. Chem.* **1998**, *22*, 693-702.
(26) Korchev, A.; Shulyak, T.; Slaten, B.; Gale, W.; Mills, G. *J. Phys. Chem. B* **2005**, *109*, 7733-7745.
(27) Khatouri, J.; Mostafavi, M.; Amblard, J.; Belloni, J. *Chem. Phys. Lett.* **1992**, *191*, 351-356.
(28) Sipos, R.; Szabo-Planka, T.; Rockenbauer, A.; Nagy, N. V.; Sima, J.; Melnik, M.; Nagypal, I. *J. Phys. Chem. A* **2008**, *112*, 10280-10286.
(29) Cadenas, E.; Packer, L. *Handbook of Antioxidants*; Marcel Dekker Inc.: Handbook of Antioxidants, 1996.
(30) Fabian, I.; Csordas, V. *Adv. in Inorg. Chem.* **2003**, *54*, 395-461.
(31) Mi, L.; Zuberbuhler, A. D. *Helv. Chim. Acta* **1992**, *75*, 1547-1556.
(32) Creutz, C. *Inorg. Chem.* **1981**, *20*, 4449-4452.
(33) Jana, N.; Gearheart, L.; Murphy, C. *Chem. Mat.* **2001**, *13*, 2313-2322.
(34) Lu, L.; Wang, H.; Zhou, Y.; Xi, S.; Zhang, H.; Jiawen, H.; Zhao, B. *Chem. Commun.* **2002**, 144-145.
(35) Hynes, M.; Kelly, D. *J. Chem. Soc., Chem. Commun.* **1988**, 849-850.
(36) Miller, D.; Buettner, G.; Aust, S. *Free Rad. Biol. Med.* **1990**, *8*, 95-108.
(37) Shtamm, E.; Purmal, A.; Skurlatov, Y. *Int. Jour. Chem. Kin.* **1979**, *11*, 461-494.

4 Conclusion

Two very different types of oxidations were investigated in this thesis. The first study involved organic oxidations. Specifically, solvent effects on antioxidant activity of a novel antioxidant, the HP-136 dimer, were assessed. The second project included an example of an inorganic oxidation reaction. The purpose of this study was to gain insight into the mechanism of copper nanoparticle (CuNP) oxidation process in order to develop strategies for CuNP stabilization under air.

The common theme of both projects was that the oxidation reactions in both cases consume molecular oxygen. This provided an opportunity to use the oxygen uptake apparatus as a key technique for studying these reactions. The oxygen uptake apparatus is a highly sensitive instrument for monitoring oxygen consumption, based on detecting changes in pressure as the reaction proceeds.

In the case of HP-136 dimer antioxidant, the oxygen uptake apparatus was employed in its traditional manner. We used the very well-established Inhibited Oxygen Uptake (IOU) method for assessing antioxidant activity.

On the other hand, using the oxygen uptake apparatus to study nanoparticle properties is something that has not been previously done. Monitoring CuNP oxidation thus constitutes a novel use of this instrument. Since then, I have helped to design oxygen uptake experiments for other projects involving nanoparticle research in the Scaiano group. Overall, it is a pleasure to see the oxygen uptake

apparatus conquering new frontiers in research. For example, we performed an experiment with a fellow graduate student, Kathy McGilvray, whose project deals with gold nanoparticles (AuNP). In this experiment, AuNP were prepared by irradiating a gold precursor salt and hydrogen peroxide (H_2O_2) solution with UVA light (Figure 4.1). In this case, the synthesis was performed directly in the oxygen uptake apparatus, with UVA irradiation through a glass window present in the body of the instrument. Evolution of O_2 was detected, and thus a hypothesized mechanism was confirmed. In an alternative experiment, performed with another graduate student, Kevin Stamplekoskie, whose research involves silver nanoparticle (AgNP) synthesis with light-emitting diodes (LED), the oxygen uptake apparatus was used to detect carbon dioxide evolution as trisodium citrate reduces AgNP in the presence of 405 nm LEDs:

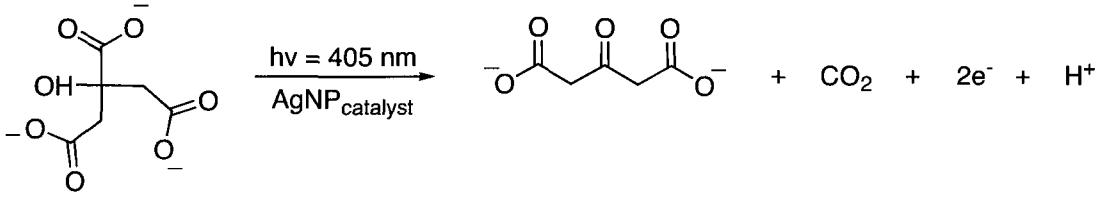

trisodium citrate

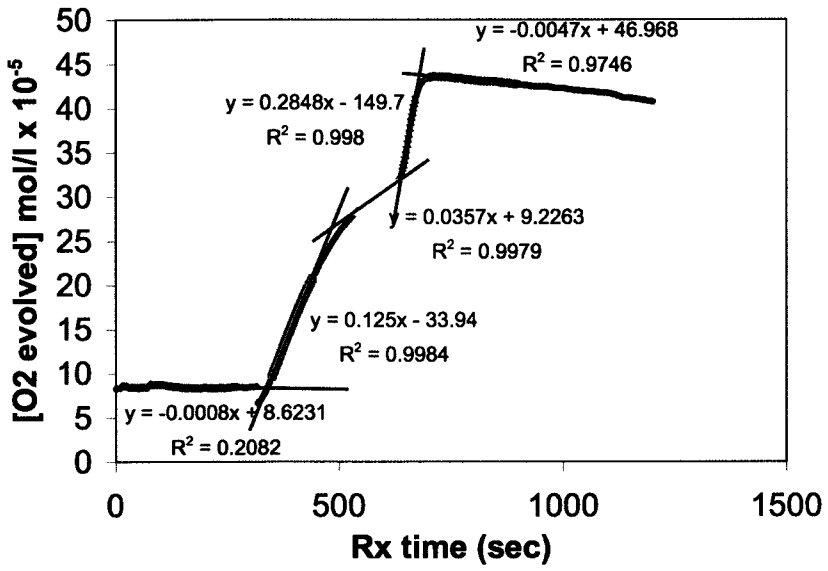

Figure 4.1 Oxygen uptake curve obtained from AuNP synthesis by UVA (350 nm) irradiation of 3 mM H_2O_2 and 0.33 mM $HAuCl_4$ in water at 30°C. Different coloured regions of the curve indicate linear regions chosen to estimate the rates of O_2 evolution during the different times of this reaction, as it proceeds.

4.1 HP-136 Dimer shows Solvent-Independent Antioxidant Activity

In chapter two of this thesis, properties of one of our newly discovered "*radically different antioxidants*", the HP-136 dimer, were investigated. This new class of chain-breaking antioxidants is very unusual because the active antioxidant species are persistent carbon-centered radicals, whereas common chain-breaking antioxidants have a phenolic structure.

The IOU method was used to determine the antioxidant activity of the HP-136 dimer in a range of solvents with varying H-bond accepting (HBA) abilities. The HP-136 dimer was found to be far less sensitive to solvent effects on antioxidant activity than a representative phenolic antioxidant, 4-methoxyphenol. In contrast to 4-methoxyphenol, the HP-136 dimer retains full antioxidant activity in HBA solvents.

This solvent-independence may provide the HP-136 dimer with an important advantage over common phenolic antioxidants in industrial applications involving polarity changes of the reaction environment. Another useful characteristic of such dimers is that they are thermally activated, which should make them even better antioxidants at higher operating temperatures.

4.2 CuNP Oxidation and Stabilization

Chapter three of this thesis describes the findings concerning CuNP oxidation. CuNP have a variety of potential applications, however instability under air is a major challenge in using CuNP at this time. The purpose of this project was to study the mechanism of CuNP oxidation in order to develop strategies for their stabilization.

The results show that under air, the CuNP oxidize within 3 hours, but the time is significantly faster with vigorous shaking. During the oxidation reaction, the CuNP were shown to form Cu^{2+} as the main product, with Cu^{+} as one of the intermediates present.

We also discovered that addition of L-ascorbic acid slowed down CuNP oxidation to ~6 hours. At the same time, the ascorbic acid is itself oxidized, and thus acts as a sacrificial stabilizer of CuNP. Our results also show that ascorbic acid reduces Cu^{2+}. We propose a mechanism of CuNP stabilization in which ascorbic acid reduces Cu^{2+} to Cu^{+}, thereby facilitating the disproportionation reaction of Cu^{+} to form more Cu^{0}. The resulting Cu^{0} may then bind to existing CuNP, thus extending their lifetime.

4.3 Future Directions

For the project involving the HP-136 dimer, it would be interesting to test its antioxidant activity at higher temperatures, perhaps at 40 or 50°C. Since these types of dimers are thermally activated, increasing the temperature would shift the equilibrium such that more dimer is present in its radical form. The observed antioxidant activity should therefore increase at higher temperatures.

It would also be of interest to perform more variable-temperature NMR experiments to see if there are certain conformations that the dimer prefers to adapt in solution at lower temperatures.

The HP-136 dimer and other similar dimers studied are insoluble in water. It would be interesting to modify the HP-136 dimer structure to make it soluble in water, to allow studies of its properties in aqueous systems. This would also open up the possibility to test the toxicity of these dimers in cells, and to assess their effect on living organisms.

For the CuNP oxidation project, a range of other antioxidants should be tested to see if they would help to stabilize CuNP.

It is also desirable to verify whether CuNP catalyze the ascorbic acid concentration, or whether residual Cu^{2+} present in the CuNP is the only species responsible. For the Cu^{2+} EPR measurements, a new flat cell should be acquired, which can be precisely repositioned into the EPR cavity during sample changes. It

would then be possible to obtain a standard curve with varying Cu^{2+} concentrations, which would allow very accurate determination of residual Cu^{2+} concentrations in CuNP solutions. If we know the residual copper (II) concentration, we could run oxygen uptake experiments in conjunction with the EPR experiment. The experiment would be similar to the one described at the end of chapter 3 of this thesis.

After CuNP stabilization is successful, an important avenue for the CuNP project would be to explore CuNP as catalysts of various reactions. Since we are a photochemistry laboratory, it would be advantageous to find a suitable photocatalytic reaction involving CuNP.

Also, it would be interesting to try to put CuNP on supports for catalysis, to see if placing the CuNP on these supports would aid in CuNP stabilization.

4.4 Publications Resulting from Work Presented in this Thesis

Filippenko, V., Frenette, M., and J.C. Scaiano. "Solvent-Independent Antioxidant Activity from Thermally Generated Carbon-Centered Radical Antioxidants", *Organic Letters*, **2009**, 11 (16), 3634-3637.